# 国家自然科学基金资助项目批准通知

张忠华　　先生/女士：

　　根据《国家自然科学基金条例》规定和专家评审意见，国家自然科学基金委员会（以下简称自然科学基金委）决定资助您申请的项目。项目批准号：52077201，项目名称：多场耦合间接/单向激励的复合双稳态多自由度压电河流俘能器研究 ， 直接费用：59.00万元，项目起止年月：2021年01月至 2024年 12月，有关项目的评审意见及修改意见附后。

　　请尽早登录科学基金网络信息系统（https://isisn.nsfc.gov.cn），获取《国家自然科学基金资助项目计划书》（以下简称计划书）并按要求填写。对于有修改意见的项目，请按修改意见及时调整计划书相关内容；如对修改意见有异议，须在电子版计划书报送截止日期前向相关科学处提出。

　　电子版计划书通过科学基金网络信息系统（https://isisn.nsfc.gov.cn）上传，依托单位审核后提交至自然科学基金委进行审核。审核未通过者，返回修改后再行提交；审核通过者，打印纸质版计划书（一式两份，双面打印），依托单位审核并加盖单位公章，将申请书纸质签字盖章页订在其中一份计划书之后，一并将上述材料报送至自然科学基金委项目材料接收工作组。电子版和纸质版计划书内容应当保证一致。**自然科学基金委将对申请书纸质签字盖章页进行审核，对存在问题的，允许依托单位进行一次修改或补齐。**

　　向自然科学基金委补交申请书纸质签字盖章页、提交和报送计划书截止时间节点如下：

　　1. **2020年10月14日16点：**提交电子版计划书的截止时间（视为计划书正式提交时间）；

　　2. **2020年10月21日16点：**提交电子修改版计划书的截止时间；

　　3. **2020年10月28日16点：**报送纸质版计划书（其中一份包含申请书纸质签字盖章页）的截止时间。

　　4. **2020年11月18日16点：**报送修改后的申请书纸质签字盖章页的截止时间。

请按照以上规定及时提交电子版计划书，并报送纸质版计划书和申请书纸质签字盖章页，未说明理由且逾期不报计划书或申请书纸质签字盖章页者，视为自动放弃接受资助；未按要求修改或逾期提交申请书纸质签字盖章页者，将视情况给予暂缓拨付经费等处理。

附件：项目评审意见及修改意见表

国家自然科学基金委员会
2020年9月18日

## 附件：项目评审意见及修改意见表

| 项目批准号 | 52077201 | 项目负责人 | 张忠华 | 申请代码1 | E0707 |
|---|---|---|---|---|---|
| 项目名称 | 多场耦合间接/单向激励的复合双稳态多自由度压电河流俘能器研究 | | | | |
| 资助类别 | 面上项目 | | 亚类说明 | | |
| 附注说明 | | | | | |
| 依托单位 | 浙江师范大学 | | | | |
| 直接费用 | 59.00 万元 | | 起止年月 | 2021年01月 至 2024年12月 | |

通讯评审意见：
<1>具体评价意见：
一、该申请项目是否面向国家需求并试图解决技术瓶颈背后的基础问题？请结合应用需求详细阐述判断理由。
自供电传感器件取代需要电池的传感器件对于环境和能源具有重要的意义，因此成为重要的研究领域。本研究面向环境监测传感器的重大需求，基于多场耦合作用构造自供电系统，具有较高的实用价值。同时本研究系统研究多场耦合作用下自激振动与能量转换的机理，理论意义也较为突出。

二、请评述申请项目所提出的科学问题与预期成果的科学价值。
本研究提出通过多场耦合作用实现流体能量转换或传递及装配预弯压电振子间接激励与单向弯曲变形发电的方法，由组合激励器与组合换能器构成复合双稳态多自由度系统，进而构造可靠性高的多自由度压电河流浮能器，切实解决相关基础理论和关键技术难题。

三、请评述申请人的研究基础及研究方案的创新性和可行性。
所提方案详细合理，采用的多物理场研究方法以及组合激励器、组合换能器都具有一定的创新性，申请人具有良好的研究积累。

四、其他建议


<2>具体评价意见：
一、该申请项目是否面向国家需求并试图解决技术瓶颈背后的基础问题？请结合应用需求详细阐述判断理由。
本项目提出通过多物理场（水流/力/磁场）耦合作用实现流体能量转换与传递和发电的新方法，通过组合激励器自激振动带动组合换能器振动发电，研究多场耦合间接激励下，组合激励器自激振动/组合换能器振动响应特性，开发高性能机电液系统，提出组合激励器自激振动产生机理及和组合换能器发电能力的形成理论，在此基础上，制备出适用于河水能量回收的微型压电发电单元和压电河流俘能器。研究项目复合国家需求，具有一定创新性。

二、请评述申请项目所提出的科学问题与预期成果的科学价值。
项目结合理论计算和仿真分析，通过多场耦合提升压电河流俘能器的性能，获得俘能器的动力学特性，关键科学问题基本合适，预期成果具有一定科学很应用家智能。

三、请评述申请人的研究基础及研究方案的创新性和可行性。
申请人前期具有一定研究基础，研究方案合理，具有可行新。

四、其他建议
预算部分太粗，材料费需要详细说明。出版/文献/信息传播/知识产权事务费中文献检索的预算费用太高。


<3>具体评价意见：
一、该申请项目是否面向国家需求并试图解决技术瓶颈背后的基础问题？请结合应用需求详细

阐述判断理由。

俘能器在河流检测领域具有重大需求，现有定向流压电俘能器存在可靠性低、流速适应性及发电能力差的缺点，不能满足市场需求。本项目拟通过构建复合双稳态多自由度系统，以解决上述问题，研究工作有市场需求牵引，研究思路具有创新性。本项目的研究目标明确，主要包括从理论上揭示机械构件与流体/磁力间的耦合作用及其对装配预弯压电振子单向弯曲振动与发电能力的影响规律，揭示多物理场耦合作用下能量转换/传递并形成装配预弯压电振子单向弯曲振动及其发电能力的机理，采用组合换能器、组合激励器和电控系统构建复合双稳态多自由度压电河流俘能器。

二、请评述申请项目所提出的科学问题与预期成果的科学价值。
本项目拟解决的科学问题凝练明晰准确，具有理论高度，将其解决能够促进压电河流俘能器的研究与开发。预期研究成果具有理论指导意义和实用价值。

三、请评述申请人的研究基础及研究方案的创新性和可行性。
申请人在俘能器研究领域具有很好的工作积累，前期研究工作有利于本项目的顺利实施。项目依托单位研究条件能够满足本项目的需求。研究内容分解详细具体，能够确保研究目标的完成。拟采用的研究方案将理论计算、仿真分析和试验测试相结合，科学合理。拟采用的技术路线可行。

四、其他建议


<4>具体评价意见：
一、该申请项目是否面向国家需求并试图解决技术瓶颈背后的基础问题？请结合应用需求详细阐述判断理由。
该项目针对目前普遍采用的定向流压电俘能器存在的可靠性低、发电能力差等问题进行研究，提出采用多物理场耦合实现流体能量转换及传递，构建复合双稳态多自由度系统。其问题的提出属于该领域的关键技术瓶颈。申请者拟通过研究组合激励器自激振动的产生机理以及环能器振动相应及发电能力的形成理论等基础问题，解决上述关键技术瓶颈。该项目的提出符合基金委"需求牵引，突破瓶颈"的要求。

二、请评述申请项目所提出的科学问题与预期成果的科学价值。
该项目拟解决的科学问题在于如何通过多物理场耦合作用实现流体能量转换与传递，进而构造多场耦合间接/单向机理的复合双稳态多自由度压电河流俘能器。其研究成果对于新型压电河流俘能器的研究与开发具有较好的推动作用。

三、请评述申请人的研究基础及研究方案的创新性和可行性。
项目申请人及其团队多年从事压电驱动控制与传感技术研究，在该领域取得了较为丰富的研究成果，研究基础较好。申请人所在单位具备开展项目研究所需的实验条件。项目的研究方案具有较好的新颖性和可行性。

四、其他建议
建议资助。


<5>具体评价意见：
一、该申请项目是否面向国家需求并试图解决技术瓶颈背后的基础问题？请结合应用需求详细阐述判断理由。
我们所处的时代能量最终会匮乏，随着人类科技活动的剧增，污染也会增加。本项目提出的压电流体俘能器研究既可以满足微功率无线监测系统的自供电需求，避免资源浪费和环境污染，又具有结构简单成本低，产生电压高的优点，将丰富的水力能源加以利用是响应时代需求，是一项面向国家有关能源、污染问题提出的举措来解决问题的新颖的科学技术。压电流体俘能器及其技术的关键之一就是转换效率，本项目即致力于该问题。

二、请评述申请项目所提出的科学问题与预期成果的科学价值。
本项目提出要解决的科学问题包括1通过理论模拟与仿真实验，获得多场耦合间接激励下装配顶弯压电振子单项弯曲振动特性及其对发电效率的影响规律 2 根据具体条件下压电振子的振动形态和形变过程设计合理的能量检测算法与控制方案。这两个问题的解决可以很好的实现俘能器有效带宽、效率和发电量的提高，是一个很好的工程问题。

三、请评述申请人的研究基础及研究方案的创新性和可行性。

有创新和可实时性，具体而实用，申请者有相关的研究基础，但从申请书中看不出来要重点解决的具体而明晰的关键自然科学问题，更多的属于工程技术问题。申请人具备仪器机械与工业自动化方面的专业背景，可以统领项目的实施；课题组其他人员专业背景和专长也可以胜任各自的科研任务。经费预算合理，人员布局和预计的工作量安排合适。

四、其他建议
1 作为一项自然科学基金，集中精力解决两项创新问题可以优质完成。
2 要实现巨大量的流体能量转换，如何恰当地提供多物理场耦合作用？

修改意见：

工程与材料科学部

2020年9月18日

# 浙江省科技计划项目

# 合 同 书

项 目 编 号： 2021C01181

项 目 名 称： 智能传感、柔性显示材料与器件研发与应
用-压电智能传感/驱动器件的关键技术研
发与应用

计 划 类 别： 省级重点研发计划

项目委托单位(甲方)： 浙江省科学技术厅

项目承担单位(乙方)： 浙江师范大学

起 止 年 月： 2021-01-01 至 2023-12-31

浙 江 省 科 学 技 术 厅

2 0 2 0 年 制

# 填 写 说 明

1. 本合同所列内容应实事求是填写，表达要明确、严谨。单位名称，请按规范全称填写，并与单位公章一致。

2. 《项目申报书》是本合同填报的重要依据，合同填报不得降低考核指标，不得自行对主要研发内容作大的调整，研发活动中如有必要变更，按照《浙江省重点研发计划暂行管理办法》（浙科发规〔2019〕110号）变更管理办理。

3. 合同中的"项目主要研发内容及创新点"，应分条目阐述拟解决的技术问题、主要创新点等，明确项目承担单位、参与单位的任务分工等。

4. 合同中的"项目研发目标及主要技术经济指标"，主要技术经济指标区分约束性指标和预期性指标。约束性指标，包括项目完成时达到的关键技术参数，技术、产品、工艺等除定量指标外还须有定性描述。预期性指标，主要指项目完成时形成的专利、论著、人才培养、产值、销售收入、利润、税收等量化指标。

5. 合同内容如涉密，应进行脱密处理，去除敏感字眼。

6. 合同中的"项目经费支出预算"应按《浙江省科技发展专项资金管理办法》（浙财科教〔2019〕7号）规定的开支范围填写。

7. 合同中的"备注"，包括重要的必须补充的内容。项目经费支出预算中有其他支出的，需在备注中明确填写支出内容。

8．合同中丙方是指项目归口管理部门，包括省有关部门和市、县科技局。市、县科技局安排项目共同支持资金的应作为合作丙方。

# 一、项目基本情况

| 项目名称 | 智能传感、柔性显示材料与器件研发与应用-压电智能传感/驱动器件的关键技术研发与应用 | 组织方式 | 竞争性项目 |
|---|---|---|---|
| 项目主管处室 | 高新处 | 项目主管 | 沈维强 |
| 项目计划类别 | 省级重点研发计划 | 项目管理领域 | 机电一体化 |
| 项目开始日期 | 2021-01-01 | 项目完成日期 | 2023-12-31 |

<table>
<tr><td rowspan="6">项目承担单位</td><td>单位名称</td><td colspan="3">浙江师范大学</td></tr>
<tr><td>单位类型</td><td>高校院所</td><td>统一社会信用代码</td><td>12330000470003513H</td></tr>
<tr><td>法人代表</td><td>郑孟状</td><td>所属行业</td><td>其他</td></tr>
<tr><td>通信地址</td><td colspan="3">金华市迎宾大道 688 号</td></tr>
<tr><td>联系人</td><td>胡瑞斌</td><td>手机</td><td>15068056698</td></tr>
</table>

| 参与单位 | | 单位名称 | 统一社会信用代码 |
|---|---|---|---|
| | 1 | 义乌清越光电科技有限公司 | 91330782MA2HR73NX2 |

鼓励在本项目实施过程中，设置科研助理岗位，聘用高校应届毕业生，预计开发科研助理岗位数 0 个，吸纳应届毕业生人数 0 人。

## 二、项目负责人及项目组成员

<table>
<tr><td rowspan="4">项目负责人</td><td>姓名</td><td>张忠华</td><td>证件号码</td><td>22072219800225421X</td></tr>
<tr><td>最高学位</td><td>博士</td><td>职称</td><td>正高级</td></tr>
<tr><td>工作单位</td><td>浙江师范大学</td><td>手机</td><td>13586979825</td></tr>
<tr><td>现从事专业</td><td>机械电子工程</td><td>年参加项目工作时间</td><td>6</td></tr>
</table>

| | 姓名 | 证件号码 | 工作单位 | 职称 | 从事专业 | 年参加项目工作时间(月) |
|---|---|---|---|---|---|---|
| 项目组成员 | 温建明 | 132628198005246111 | 浙江师范大学 | 正高级 | 机械电子工程 | 6 |
| | 阚君武 | 220104196509285539 | 浙江师范大学 | 正高级 | 机械设计及理论 | 6 |
| | 马继杰 | 120225198012201013 | 浙江师范大学 | 副高级 | 机械电子工程 | 6 |
| | 穆欣炬 | 65292519761119001X | 义乌清越光电科技有限公司 | 其他 | 电子工程 | 3 |
| | 王淑云 | 220104196502021549 | 浙江师范大学 | 正高级 | 应用数学 | 6 |
| | 浦斌 | 320583198510223837 | 义乌清越光电科技有限公司 | 其他 | 电子工程 | 3 |
| | WANG LINLIN | AC747687 | 浙江师范大学 | 副高级 | 材料工程 | 6 |
| | 张昱 | 330726197911041111 | 浙江师范大学 | 中级 | 机械电子工程 | 6 |
| | 陈松 | 362202198809057313 | 浙江师范大学 | 副高级 | 机械设计及理论 | 6 |
| | 李建平 | 32030519870617001X | 浙江师范大学 | 中级 | 机械设计及理论 | 6 |

| 胡意立 | 330184198903250031 | 浙江师范大学 | 中级 | 机械设计及理论 | 6 |
|---|---|---|---|---|---|
| 蒋永华 | 330681198204050493 | 浙江师范大学 | 副高级 | 机械电子工程 | 4 |
| 孙建飞 | 530323198406040776 | 义乌清越光电科技有限公司 | 其他 | 电子工程 | 3 |
| 唐鹏宇 | 3212021993051700lX | 义乌清越光电科技有限公司 | 其他 | 电子工程 | 4 |
| 马中生 | 320382198802165758 | 义乌清越光电科技有限公司 | 其他 | 电子工程 | 6 |
| 吕鹏 | 330624199510232057 | 浙江师范大学 | 其他 | 机械工程 | 8 |
| 王进 | 331021199708052034 | 浙江师范大学 | 其他 | 机械工程 | 8 |
| 杨泽盟 | 130302199701263946 | 浙江师范大学 | 其他 | 机械工程 | 8 |
| 张敏 | 530302199702053021 | 浙江师范大学 | 其他 | 机械工程 | 8 |
| 林仕杰 | 330381199612263314 | 浙江师范大学 | 其他 | 机械工程 | 8 |
| 唐红艳 | 522321199610091644 | 浙江师范大学 | 其他 | 机械工程 | 8 |
| 柴超辉 | 330821199607066691 | 浙江师范大学 | 其他 | 机械工程 | 8 |
| 陆奇涛 | 3304811996l026321X | 浙江师范大学 | 其他 | 机械工程 | 8 |
| 何立栋 | 330621199707297410 | 浙江师范大学 | 其他 | 机械工程 | 8 |
| 林圣荣 | 450821200005012541 | 浙江师范大学 | 其他 | 机械工程 | 8 |

| 葛程鹏 | 331082199802129053 | 浙江师范大学 | 其他 | 机械工程 | 8 |
| 沈国成 | 330724199712195413 | 浙江师范大学 | 其他 | 机械工程 | 8 |
| 刘海东 | 612425199704270013 | 浙江师范大学 | 其他 | 机械工程 | 8 |
| 张杰 | 342622199612074310 | 浙江师范大学 | 其他 | 机械工程 | 8 |

## 三、项目主要研发内容及创新点

主要研究内容：（1）压电传感/驱动器件双向贯通共性理论及机-力-电-液-磁的多场耦合机理研究，利用 ANSYS、COMSOL 等工具进行模拟与仿真分析，从理论上获得机-力-电-液-磁间的多场耦合规律以及合理的系统参数匹配关系，为系统总体的协同设计提供理论依据；（2）压电式自驱动传感器的多维耦合振动能量收集研发，利用磁力耦合使悬吊式质量块上的磁铁与悬臂梁压电振子端部磁铁产生相互作用，通过任意方向振动引起悬吊式磁铁的位置变化使压电振子受力状态改变，从而将机械能转换成电能；（3）压电-流体耦合式振动能量收集器的研发，研究压电-流体耦合式振动能量收集器中机电液系统的耦合关系，建立压电振子、液体及振动负荷间耦合作用的动力学模型，研究基于同步开关能量回收技术的振动系统，分析开关控制策略/电路形式/器件参数等对机械单元响应特性及频带宽度（即环境适应能力）的影响规律；（4）驱控一体化压电惯性精密驱动器的研发，研究所提出的驱动一体化压电惯性精密驱动器的作用机理、耦合特性、响应特性及其控制策略，构造不同类型、高精度、驱动能力强、集成化的驱控一体化压电惯性精密驱动器；（5）自检测/自激励压电尺蠖驱动器运动机理及耦合特性研究，研究采用永磁体作为箝位元件，对滑块进行箝位，将原有的接触式箝位转换为磁力非接触式箝位；利用激光对射传感器将永磁体位置检测信号转化为压电叠堆的激励信号，实现机构自激励的新方法；(6)原位生长织构化无铅压电陶瓷薄膜的制备和性能研究，利用一维纳米结构压电陶瓷材料柔韧性好，临界应变值大，受力变形的敏感性好的优势，拟采用液相反应方法，在金属表面原位生长具有一维纳米阵列结构的高性能无铅钙钛矿类压电薄膜；（7）压电智能传感/驱动器件的示范应用，开发和研制出面向自驱动主动式传感的压电俘能器、驱控一体化压电精密驱动器、自检测/自激励压电尺蠖驱动器，以能量密度、能量转换效率、分辨率为关键指标进行测试，根据样机测试结果，进一步优化加工工艺、结构设计和材料匹配，最终形成产品的性能检测、生产示范和使用示范报告。

主要创新点：（1）国内率先提出压电传感器与驱动器的双向贯通共性理论，开发一套机-力-电-液-磁多场耦合机理的仿真体系，逐步建立物性型传感器与执行器统一理论体系框架，为压电传感器/驱动器集成化与一体化以及同位信号的融合、解耦与分离奠定坚实理论基础；（2）提出利用弹簧牵吊质量块感知多维振源振动、并通过非接触磁力激励压电振子发电，实现任意方向的振动能量收集，通过低刚度弹簧和大质量块降低系统固有频率，实现不以降低系统可靠性为代价的低频振动能量收集，突破压电能量收集器同时实现低频与多方向振动收集的技术；（3）采用液相反应方法，在金属表面原位生长具有一维纳米阵列结构的高性能无铅钙钛矿类织构化薄膜，提供一种适于柔性显示器、电子纸、可穿戴设备等领域的压电薄膜材料，简化了压电元件制造过程，提高了钙钛矿基薄膜的形状适应性、柔韧性和压电性，突破钙钛矿基薄膜压电性与柔韧性改进的"卡脖子"技术。

任务分工：根据项目目标、主要研究内容、技术路线和工艺流程，为提高项目实施效

2021/05/11 1620696462515

率，做到有效监控，同时也为充分发挥各项目实施单位的技术特点和优势，将本项目分解为 5 个子课题：（1）压电传感器与驱动器的共性理论以及机-力-电-液-磁的多场耦合机理研究，高校牵头，企业配合；（2）压电步进式精密驱动器研究，高校牵头，企业配合；（3）振动压电能量回收器研究，高校牵头，企业配合；（4）织构化压电陶瓷薄膜制备研究，高校牵头，企业配合；（5）压电智能传感/驱动器件的示范应用，企业牵头，高校提供技术支持。

# 四、项目研发目标及主要技术经济指标

## 1. 研发目标

一、研发主要针对的问题和需求：（1）现有压电振动能量采集器自身频带窄、固有频率高及振动能量收集方向单一；（2）压电驱动器尚存在尺寸大、驱动能力不足、难于集成化等难题；（3）压电薄膜材料压电系数低、柔韧性差造成压电元件灵敏度小和可靠性低。　二、拟解决或突破的关键核心技术：（1）压电低频多维振动能量收集器的机械单元与电控单元工作协同；（2）提高压电-流体耦合式振动能量收集系统的机械单元响应特性；（3）压电惯性精密驱动器的驱动和箝位动作自动匹配；（4）压电叠堆驱动与永磁体控制多场耦合规律以及驱动控制的形成机理和方法；（5）压电薄膜在水热或微弧氧化反应过程中保持一维纳米结构不坍塌。　三、预期成果：全面掌握压电智能传感/驱动核心技术，完全拥有自主知识产权。　　　四、成果应用形式：通过义乌清越光电科技有限公司的示范应用测试成功后，将进一步推广应用于母公司维信诺等企业，带动整个产业转型提升，确保产业链安全。　　　五、预期标志性成果及形成时间：项目执行期内，实现压电薄膜材料、压电能量收集/精密驱动装置自主知识产权，申请发明专利 10 件以上，发表学术论文 15 篇以上。　六、知识产权 ：通过本项目的研究实施，将在压电柔性薄膜材料、压电能量收集/精密驱动装置新型结构及加工工艺、多物理场耦合测试试验台及评价方法、关键部件表面加工方法等方面申请发明专利 10 件以上，并实现专利转化 2 项以上，研制各类样机 15 台/套。　七、学术论文：围绕压电智能传感/驱动三大关键技术压电柔性薄膜材料、压电能量收集、压电精密驱动机-力-电-液-磁耦合模型及求解方法、新型柔性薄膜研发、集成化一体化设计、结构优化等方面发表学术论文 15 篇以上，其中 SCI TOP 论文 6 篇以上，国内顶级期刊（机械工程学报、中国电机工程学报、振动工程学报等）4 篇以上。

## 2. 约束性指标

针对压电智能传感与驱动行业关键技术柔性材料/能量收集/精密驱动的设计、制造及示范应用，主要达到以下指标：

（1）压电精密驱动直线运动分辨率≤0.02μm；

（2）压电精密驱动承载承载≥500g，驱动力≥100g；

（3）压电能量收集输出电压：≥50 V；

（4）压电能量收集输出功率：≥1 mW；

（5）实现一维纳米阵列结构的高性能无铅钙钛矿类压电薄膜的制备；

（6）实现压电能量收集/精密驱动集成化一体化设计，内置信号发生器与功率放大器等功能；

量化指标

获得目标战略产品(新产品、新工艺)__5__项；解决关键共性技术__2__项；示范工程、示范点__1__个；开发样机：__15__台套；突破卡脖子关键瓶颈技术：__3__项。

3. 预期性指标

预计项目完成时：

1. 申请专利__10__项，其中发明专利 __10__件（国内发明专利 __10__件，PCT/EPO 专利 __0__件）；授权专利__10__件，其中授权发明专利 __10__件（国内发明专利 __10__件，PCT/EPO 专利 __0__件）。

2. 参与制订标准__0__项，其中：国际标准__0__项，国家标准__0__项，地方标准__0__项，行业标准__0__项）。

3. 获得软件著作权__0__项。

4. 发表高水平论文__15__篇，其中：SCI 收录论文__10__篇，EI 收录论文__5__篇，国内核心期刊论文__5__篇；出版论著 __0__部。

5. 培养硕士或博士研究生__10__名，其中博士__0__名；职称晋升__4__人，其中：晋升正高级职称__1__人，副高级职称__3__人。

6. 项目执行期间累计实现产值 __1000__万元，销售收入__1000__万元，利润 __100__万元，上缴税金__25__万元。

7. 其他：_____ 。

2021/05/11 1620696462515

## 五、计划进度目标

| 起止年月 | | | 考核指标 | 成果形式 |
|---|---|---|---|---|
| 2021-01-01 | 至 | 2021-12-31 | ◇确定总体研究方案，搭建压电传感/驱动等检测试验台；◇开展子课题1研究，针对压电传感器/驱动器的双向贯通共性理论开展建模与多物理场耦合分析；◇申报国家发明专利3项，撰写高水平学术论文5篇。 | 专利、论文 |
| 2022-01-01 | 至 | 2022-12-31 | ◇开展子课题2、3、4研究；◇完成驱动与控制系统的设计与制作，完成数据采集及测试分析系统的制作、编程及调试；◇申报国家发明专利3项，撰写高水平学术论文5篇。 | 论文、专利、样机 |
| 2023-01-01 | 至 | 2023-12-31 | ◇开展子课题5研究，完成样机的制作；◇继续完善和优化各子课题内容，实现驱动与控制一体化、集成化设计；◇总结形成关键技术文件，撰写研究工作的结题报告；◇申报国家发明专利4项，撰写高水平学术论文5篇。 | 论文、专利、样机 |

注：如为预期里程碑式成果形成节点，请在"成果形式"栏标注"里程碑式成果"

## 六、项目经费来源

1、本项目研发总经费 <u>1000</u> 万元，其中：甲方补助 <u>390</u> 万元，乙方自筹 <u>610</u> 万元，丙方共同支持 <u>0</u> 万元。

2、甲方经费拨付计划（参与单位经费由承担单位转拨）

单位：万元

|  | 首期 | 二期 | 三期 | 合计 |
|---|---|---|---|---|
| 甲方资金 | 234 | 156 | 0 | 390 |

|  | 甲方补助 | 承担单位 | 参与单位1 |
|---|---|---|---|
| 首期 | 234 | 187.2 | 46.8 |
| 二期 | 156 | 124.8 | 31.2 |
| 三期 | 0 | 0 | 0 |
| 合计 | 390 | 312 | 78 |

3、乙方自筹和共同支持资金到位计划

单位：万元

|  | 首期 | 二期 | 三期 | 合计 |
|---|---|---|---|---|
| 乙方自筹资金 | 210 | 200 | 200 | 610 |
| 丙方共同支持资金 | 0 | 0 | 0 | 0 |

|  | 乙方自筹 | 承担单位 | 参与单位1 |
|---|---|---|---|
| 首期 | 210 | 100 | 110 |
| 二期 | 200 | 100 | 100 |
| 三期 | 200 | 100 | 100 |
| 合计 | 610 | 300 | 310 |

|  | 丙方共同支持 | 承担单位 | 参与单位1 |
|---|---|---|---|
| 首期 | 0 | 0 | 0 |
| 二期 | 0 | 0 | 0 |
| 三期 | 0 | 0 | 0 |
| 合计 | 0 | 0 | 0 |

2021/05/11 1620696462515

# 七、项目经费支出预算

| | 经费开支科目 | 预算经费总额 | 其中省财政经费 |
|---|---|---|---|
| 一 | 直接费用 | 900 | 340 |
| 1 | 设备费 | 310 | 40 |
| 2 | 材料费 | 290 | 145 |
| 3 | 测试化验加工费 | 80 | 60 |
| 4 | 燃料动力费 | 0 | 0 |
| 5 | 差旅/会议/国际合作与交流费 | 80 | 20 |
| 6 | 出版/文献/信息传播/知识产权事务费 | 15 | 5 |
| 7 | 劳务费 | 120 | 70 |
| 8 | 专家咨询费 | 5 | 0 |
| 9 | 其他支出 | 0 | 0 |
| 二 | 间接费用 | 100 | 50 |
| 10 | 间接费用(包含管理费与激励费) | 100 | 50 |
| | 合计（请保留整数） | 1,000 | 390 |

## 八、需增添的科研仪器及设备（单价 50 万元及以上分栏填写，单价 50 万元以下仪器统一在"其他"栏）

:

| 名 称 | 数 量 | 单价（万元） | 省科技厅拨款（万元） | 自筹（万元） | 用途说明 |
|---|---|---|---|---|---|
| 其他 | 9 | -- | 40 | 270 | 柔性电子纸制备<br>信号发生器、功率放大器、振动台 |
| 合计 | -- | -- | 40 | 270 | -- |

注：财政经费不得用于购置生产设备、生产及科研共用设备及通用办公设备，只能用于购置本项目专用的科研仪器设备。

2021/05/11 1620696462515

# 合 同 其 他 条 款

1. 各方应严格遵守本合同的各项条款。因合同执行过程中出现的客观原因，任何一方认为有必要变更合同条款内容的，需经协商一致。

2. 乙方应按《浙江省科技发展专项资金管理办法》（浙财科教〔2019〕7号）规定，按经费来源分别对经费支出单独建账，独立核算，专款专用。

3. 甲方有权按照合同的要求，监督、检查乙方项目进展和经费使用情况，乙方应予以配合。乙方应按照《浙江省重点研发计划暂行管理办法》（浙科发规〔2019〕110号）规定，按时向甲方报送项目执行、变更和经费使用情况。

4. 乙方应按照合同的要求组织实施项目、使用项目经费。乙方未按本合同落实自筹经费，或未按规定使用项目经费的，甲方有权暂停拨款直至解除合同，并收回已投入的经费。

5. 丙方应协助甲方监督、检查乙方项目进展和经费使用情况，协调解决合同执行过程中出现的问题。合同履行过程中，如丙方发现乙方存在或可能存在无力或不愿忠实履行合同义务情形时，应及时向甲方提出暂停拨款或解除合同等建议。

6. 乙方由多家单位组成的，各方的出资数额、方式、时间以及其他相关权利和义务需单独订立协议。

7. 根据《浙江省科技计划（专项、基金）项目验收管理办法》（浙科发计〔2017〕146号），乙方完成本项目任务后，应及时提交相关材料，做好验收工作。

8. 成果的权属和保密。本项目研究取得的技术成果，其知识产权归属及成果转化，按国家和本省的有关规定执行。涉及国家机密的，按国家《中华人民共和国保守国家秘密法》和《科学技术保密规定》有关规定执行。

9. 本合同文本一式六份，经三方加盖公章后生效，分存甲方、乙方、丙方及有关单位。

甲方(项目委托单位)： (盖章)

单位负责人（签字）：

年 月 日

乙方（项目承担单位）： (盖章)

项目（课题）负责人（签字）：

单位负责人（签字）：

年 月 日

丙方(项目归口管理责任部门)： (盖章)

单位负责人（签字）：

单位地址：

联系电话

年 月 日

# 发明专利证书

发 明 名 称：一种磁耦合非共振旋转压电发电机

发 明 人：张忠华;吕鹏;万嫩;阚君武;王淑云;张昱;程光明;林仕杰

专 利 号：ZL 2019 1 0120777.4

专利申请日：2019 年 01 月 30 日

专 利 权 人：浙江师范大学

地 址：321004 浙江省金华市婺城区迎宾大道 688 号浙江师范大学

授权公告日：2020 年 07 月 07 日  授权公告号：CN 109756153 B

　　国家知识产权局依照中华人民共和国专利法进行审查，决定授予专利权，颁发发明专利证书并在专利登记簿上予以登记。专利权自授权公告之日起生效。专利权期限为二十年，自申请日起算。

　　专利证书记载专利权登记时的法律状况。专利权的转移、质押、无效、终止、恢复和专利权人的姓名或名称、国籍、地址变更等事项记载在专利登记簿上。

局长
申长雨

2020 年 07 月 07 日

其他事项参见背面

# 发明专利证书

发 明 名 称： 一种步进式气缸

发 明 人： 张忠华;林仕杰;刘立博;柴君凌;汪彬;曾平

专 利 号： ZL 2019 1 0166692.X

专 利 申 请 日： 2019 年 03 月 01 日

专 利 权 人： 浙江师范大学

地 址： 321004 浙江省金华市婺城区迎宾大道 688 号浙江师范大学

授权公告日： 2020 年 07 月 28 日 授权公告号： CN 109882470 B

　　国家知识产权局依照中华人民共和国专利法进行审查，决定授予专利权，颁发发明专利证书并在专利登记簿上予以登记。专利权自授权公告之日起生效。专利权期限为二十年，自申请日起算。

　　专利证书记载专利权登记时的法律状况。专利权的转移、质押、无效、终止、恢复和专利权人的姓名或名称、国籍、地址变更等事项记载在专利登记簿上。

局长
申长雨

2020 年 07 月 28 日

其他事项参见背面

证书号第4002734号

# 发明专利证书

发　明　名　称：一种自驱动液压缸

发　明　人：张忠华;柴君凌;黄鑫;温建明;王成武;林仕杰

专　利　号：ZL 2019 1 0166604.6

专利申请日：2019年03月01日

专　利　权　人：浙江师范大学

地　　　　址：321004 浙江省金华市婺城区迎宾大道688号浙江师范大学

授权公告日：2020年09月25日　　　　授权公告号：CN 109826842 B

　　国家知识产权局依照中华人民共和国专利法进行审查，决定授予专利权，颁发发明专利证书并在专利登记簿上予以登记。专利权自授权公告之日起生效。专利权期限为二十年，自申请日起算。

　　专利证书记载专利权登记时的法律状况。专利权的转移、质押、无效、终止、恢复和专利权人的姓名或名称、国籍、地址变更等事项记载在专利登记簿上。

局长　申长雨

2020年09月25日

第1页（共2页）

其他事项参见背面

证书号第 4121236 号

# 发明专利证书

发 明 名 称：一种气动输液装置

发 明 人：张忠华;柴君凌;杨普雄;李建平;林仕杰;曾平

专 利 号：ZL 2019 1 0166605.0

专利申请日：2019 年 03 月 01 日

专 利 权 人：浙江师范大学

地 址：321004 浙江省金华市婺城区迎宾大道 688 号浙江师范大学

授权公告日：2020 年 11 月 27 日  授权公告号：CN 109771740 B

　　国家知识产权局依照中华人民共和国专利法进行审查，决定授予专利权，颁发发明专利证书并在专利登记簿上予以登记。专利权自授权公告之日起生效。专利权期限为二十年，自申请日起算。

　　专利证书记载专利权登记时的法律状况。专利权的转移、质押、无效、终止、恢复和专利权人的姓名或名称、国籍、地址变更等事项记载在专利登记簿上。

局长
申长雨

2020 年 11 月 27 日

第 1 页 (共 2 页)

其他事项参见续页

证 书 号 第 4121236 号

专利权人应当依照专利法及其实施细则规定缴纳年费。本专利的年费应当在每年 03 月 01 日前缴纳。未按照规定缴纳年费的，专利权自应当缴纳年费期满之日起终止。

申请日时本专利记载的申请人、发明人信息如下：

申请人：

　　　　浙江师范大学

发明人：

　　　　张忠华；柴君凌；杨普雄；李建平；林仕杰；曾平

# 发明专利证书

发 明 名 称：一种气体混合器

发 明 人：张忠华;林仕杰;刘立博;阚君武;张敏;曾平

专 利 号：ZL 2019 1 0166693.4

专 利 申 请 日：2019 年 03 月 01 日

专 利 权 人：浙江师范大学

地 址：321004 浙江省金华市婺城区迎宾大道 688 号浙江师范大学

授权公告日：2021 年 03 月 02 日 授权公告号：CN 109772222 B

国家知识产权局依照中华人民共和国专利法进行审查，决定授予专利权，颁发发明专利证书并在专利登记簿上予以登记。专利权自授权公告之日起生效。专利权期限为二十年，自申请日起算。

专利证书记载专利权登记时的法律状况。专利权的转移、质押、无效、终止、恢复和专利权人的姓名或名称、国籍、地址变更等事项记载在专利登记簿上。

局长
申长雨

2021 年 03 月 02 日

证书号第 4277756 号

专利权人应当依照专利法及其实施细则规定缴纳年费。本专利的年费应当在每年 03 月 01 日前缴纳。未按照规定缴纳年费的，专利权自应当缴纳年费期满之日起终止。

申请日时本专利记载的申请人、发明人信息如下：

申请人：

　　浙江师范大学

发明人：

　　张忠华；林仕杰；刘立博；阚君武；张敏；曾平

证书号第4294002号

# 发 明 专 利 证 书

发 明 名 称：一种压电堆驱动的输液装置

发 明 人：张忠华;陈泽锋;唐姣;王淑云;温建明;杨泽盟

专 利 号：ZL 2019 1 0166691.5

专利申请日：2019 年 03 月 01 日

专 利 权 人：浙江师范大学

地 址：321004 浙江省金华市婺城区迎宾大道 688 号浙江师范大学

授权公告日：2021 年 03 月 12 日　　　授权公告号：CN 109821093 B

　　国家知识产权局依照中华人民共和国专利法进行审查，决定授予专利权，颁发发明专利证书并在专利登记簿上予以登记。专利权自授权公告之日起生效。专利权期限为二十年，自申请日起算。

　　专利证书记载专利权登记时的法律状况。专利权的转移、质押、无效、终止、恢复和专利权人的姓名或名称、国籍、地址变更等事项记载在专利登记簿上。

局长
申长雨

2021 年 03 月 12 日

证 书 号 第 4294002 号

专利权人应当依照专利法及其实施细则规定缴纳年费。本专利的年费应当在每年 03 月 01 日前缴纳。未按照规定缴纳年费的，专利权自应当缴纳年费期满之日起终止。

申请日时本专利记载的申请人、发明人信息如下：
申请人：
　　　　浙江师范大学

发明人：
　　　　张忠华;陈泽锋;唐姣;王淑云;温建明;杨泽盟

证书号第 4304436 号

# 发明专利证书

发 明 名 称：一种压电片驱动的注射系统

发 明 人：张忠华;林仕杰;陈泽锋;王淑云;马继杰;杨泽盟

专 利 号：ZL 2019 1 0166694.9

专利申请日：2019 年 03 月 01 日

专 利 权 人：浙江师范大学

地 址：321004 浙江省金华市婺城区迎宾大道 688 号浙江师范大学

授权公告日：2021 年 03 月 16 日　　　　授权公告号：CN 109876239 B

　　国家知识产权局依照中华人民共和国专利法进行审查，决定授予专利权，颁发发明专利证书并在专利登记簿上予以登记。专利权自授权公告之日起生效。专利权期限为二十年，自申请日起算。

　　专利证书记载专利权登记时的法律状况。专利权的转移、质押、无效、终止、恢复和专利权人的姓名或名称、国籍、地址变更等事项记载在专利登记簿上。

局长
申长雨

2021 年 03 月 16 日

证书号第 4304436 号

专利权人应当依照专利法及其实施细则规定缴纳年费。本专利的年费应当在每年 03 月 01 日前缴纳。未按照规定缴纳年费的，专利权自应当缴纳年费期满之日起终止。

申请日时本专利记载的申请人、发明人信息如下：

申请人：

浙江师范大学

发明人：

张忠华;林仕杰;陈泽锋;王淑云;马继杰;杨泽盟
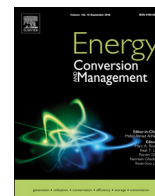
# A pneumatic piezoelectric vibration energy harvester based on the compressed air-transducer-structure interaction

Zhonghua Zhang[a,b], Shuyun Wang[a,b,*], Junwu Kan[a,b], Wenjing Hu[c], Zefeng Chen[a,b], Hailong Xu[a]

[a] *Key Laboratory of Urban Rail Transit Intelligent Operation and Maintenance Technology and Equipment of Zhejiang Province, Zhejiang Normal University, Jinhua 321004, PR China*
[b] *Collaboration and Innovation Center for Urban Rail Transit Operation Safety Technology and Equipment of Zhejiang Province, Zhejiang Normal University, Jinhua 321004, PR China*
[c] *College of Applied Technology, Dalian Ocean University, Dalian 116300, PR China*

ABSTRACT

Harvesting energy from the ambient vibration to replace the conventional electrochemical batteries has gained considerable interest. Different from the most existing flow-induced vibration energy harvesters based on the continuous airflow, by using the pressure energy of the air rather than the kinetic energy, a novel pneumatic piezoelectric vibration energy harvester (PVEH) based on compressed air-transducer-structure interaction is presented and fabricated in this paper. To verify the feasibility of the proposed principle and design, the experiments of frequency responses were performed to evaluate the energy harvesting performance in terms of vibrational displacement and open-circuit voltage. It was found that the power generation characteristics of the pneumatic PVEH was almost totally independent of the vibration properties because of the mutual interaction between the compressed air, piezoelectric transducer and damping orifice. Experimental results demonstrated there was an optimal proof mass of 12.5 kg to maximize the open-circuit voltage for this prototype PVEH. The optimal excitation frequency of the voltage-frequency response decreased linearly with the rising air pressure. With the enhancement of the initial air pressure from 0.1 MPa to 0.95 MPa, the optimal frequency was dropped from 55 Hz to 31 Hz. The open-circuit voltage could be improved through reducing the size of damping orifice, where the output voltage reached the maximum value of 51.6 V at the air pressure of 0.5 MPa with the valve opening of 1/6. Besides, more than one peak voltage would occur with the increase of the air pressure or the size of the damping orifice. It is expected that this study can provide a guideline for the design and application of the PVEH using the compressed air.

## 1. Introduction

Energy harvesting from ambient vibration by using piezoelectric mechanism has attracted increasing attention to replace the conventional electrochemical batteries because piezoelectric transduction has high power density, high energy conversion efficiency and ease of fabrication and implementation [1–4]. Many types of piezoelectric vibration energy harvesters (PVEHs) were presented and developed to harvest the surrounding available vibration sources, such as moving vehicles, passing trains, ocean waves, transportation infrastructure, human motion, machinery equipment, engine and raindrop [5–10]. In order to harvest these ambient vibrations effectively, various structures and configurations of the PVEHs are presented. For instance, cantilever-type [11–14], disk-type [15–17], stack-type [18–20], cymbal-type [21–23] and bridge-type [24,25]. A variety of piezoelectric materials

are applied in these PVEHs, including piezoelectric ceramics (PZT) [2–5,26–28], piezoelectric polymer (PVDF) [29–31], aluminum nitride (AlN) [32–34], macro fiber composite (MFC) [35–37] and ZnO thin film [38,39].

Not only ambient vibrations, but also some other forms of environmental energies like wind and water were frequently transformed into the kinetic energy of the vibration to further generate the electricity based on the piezoelectric mechanism [40–43]. As a result, piezoelectric energy harvesting from flow-induced vibrations, e.g., vortex-induced [44,45], turbulence-induced [46,47] and galloping vibrations [48,49], has become an interesting research topic in the field of renewable energy sources. Mutsuda et al. proposed a highly flexible piezoelectric energy device to harvest flow-induced vibration such as ocean and wind energy [50]. Li et al. reviewed the design, implementation, and demonstration of energy harvesting devices that

exploited flow-induced vibrations in aerospace engineering [51]. Truitt and Mahmoodi reviewed piezoelectric wind energy harvesters based on the vortex-induced vibration, galloping, flutter and buffeting [48,52]. Hu et al. established a three-field coupling model for a vortex shedding-induced piezoelectric energy harvester [44]. Hobeck and Inman developed a kind of artificial piezoelectric grass for low-velocity, highly turbulent fluid flow environments like streams or ventilation systems [53]. Tsujiura et al. developed a piezoelectric energy harvester of the PZT thin-film bimorph cantilever utilizing the self-excited vibration induced by uniform airflow [54]. A brief survey of literatures shows that researchers have already conducted a large body of work on piezoelectric energy harvesters using the flow-induced vibrations. Meanwhile, it is noticed that almost all of flow-induced vibration energy harvesters were induced by the continuous airflow, namely kinetic energy of the air. It is generally known that the fluid has three different forms of energies: kinetic energy, potential energy and pressure energy. In contrast, very few piezoelectric energy harvesters to date were developed using the compressed air, which could be applied in many circumstances. For example, pneumatic suspension systems powered by the compressed air were massively exploited in railway vehicles, coaches, limousines, trucks and trailers [55–58]. However, up to now there are rather few reports on the PVEHs available for the pneumatic systems. If the vibration energy in these scenarios mentioned above could be harvested and further transformed into electric energy to construct semi-active pneumatic components, the effectiveness of the vibration control and suppression would be further improved.

Different from the aforementioned piezoelectric energy harvesters using the continuous airflow, this paper presents a pneumatic piezoelectric vibration energy harvester based on compressed air-transducer-structure interaction. The compressed air was used as the transferring media to realize the energy conversion from the kinetic energy of the vibration to the electric energy. So another difference from the previous most PVEHs was that the piezoelectric element of the proposed PVEH was not directly subjected to the vibration sources. The configuration and principle of the pneumatic PVEH was introduced and a prototype PVEH was fabricated to verify the feasibility by the experimental frequency responses. The influence of several key structural parameters on the performance of the pneumatic PVEH was tested and analyzed.

As illustrated in Fig. 1, the pneumatic PVEH is composed of a double-acting air piston cylinder, a balance spring in parallel with the cylinder, a proof mass bond to the piston, a damping orifice and piezoelectric transducers. The rod and non-rod chambers of the cylinder were connected by the damping orifice. A round piezoelectric diaphragm with clamped edges divided the piezoelectric transducer into two symmetrical cavities which were respectively connected with both chambers of the cylinder. In general, the cylinder is positioned between the vibration part and main body in pneumatic suspension/isolation/

shock absorption systems. While the cylinder vibrated with the excitation sources, it would lead to a relative displacement between the piston and cylinder body owing to the inertia. Consequently, the piston bond to the proof mass forced the air medium to be further compressed, meanwhile, the compressed air flowed between two chambers via the damping orifice. When the air moved from one end of the orifice to the other end, the pressure loss was caused due to the frictional resistance along the track. So the pressure difference would occur between upper and lower chambers of the cylinder when the piston was moved by the vibration. Since the cylinder chambers were connected with the transducer cavities respectively, the same pressure difference was applied on both surfaces of the piezoelectric disks. Then piezoelectric elements produced the bending deformation and electric energy was thus generated under the alternating pressure due to the direct piezoelectric effect.

The working process demonstrated that the generated electric energy was not directly caused by the vibration. For the presented PVEH, the vibration resulted in an inertial force of the proof mass, whose direct effect was to further compress and drive the air. Because of the damping orifice, the pressure difference between two cylinder chambers was induced when the compressed air was forced to flow between both chambers. It was the pressure difference that brought about the bending vibration of the piezoelectric diaphragm and thus electric energy was generated under the deformation. In summary, the kinetic energy of the vibration was firstly converted into the pressure energy of the air and then it was transformed into the electric energy of the piezoelectric transducer. Accordingly, a pneumatic PVEH was realized through the interaction of the compressed air, the damping orifice and the piezoelectric transducer, meanwhile, it was also the main novelty of this work. To the authors' knowledge, this is the first time that a PVEH has been developed by using the compressed air-piezoelectric transducer-damping orifice interaction. The proposed PVEH was different from the most existing both vibration-based and flow-induced energy harvesters. Although the pneumatic PVEH was essentially still a kind of vibration-based energy harvester, it was significantly different from the most PVEHs in which the vibration source applied directly on the piezoelectric element. Besides, there was an essential difference between the presented PVEH and flow-induced vibration energy harvesters. As a type of vibration-based energy harvester, the proposed PVEH converted the vibration energy into electric energy. The compressed air inside the pneumatic PVEH was only the intermediate transferring medium, through which the PVEH realized the energy conversion from mechanical vibration to electric energy. In contrast, the air or water was a main power source for existing flow-induced vibration energy harvesters, where the kinetic energy of the fluid was directly transformed into electric energy.

On one hand, the piezoelectric transducer of the presented PVEH
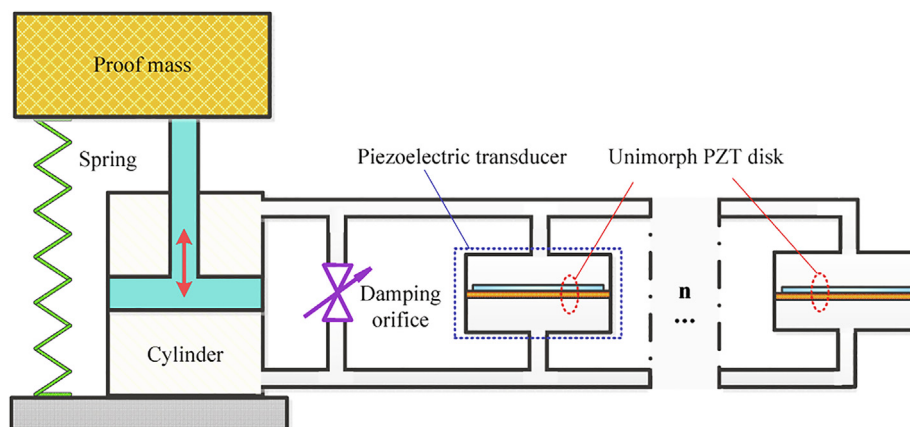


**Fig. 1.** Schematic illustration of the pneumatic PVEH based on compressed air-transducer-structure interaction.
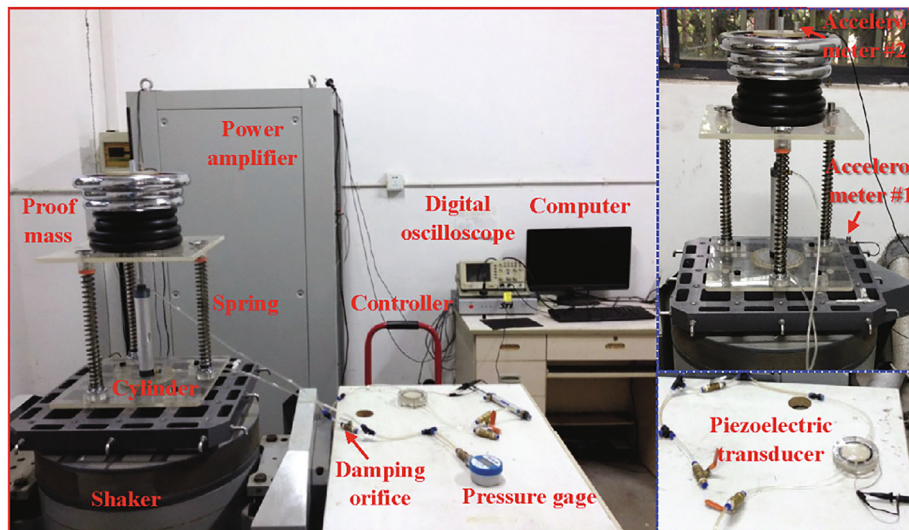
Fig. 2. The schematic diagram of the experimental setup.

did not directly vibrated with the excitation source. The vibration, which was transferred to the proof mass bond to the cylinder piston might have been considerably different from the excitation source because of the interaction between the vibrating proof mass, the compressed air and the damping orifice. Intuitively, the vibration transfer was greatly influenced by the above factors. For example, it is well known that the air viscosity increases as the pressure rises as well as the fluid movement is strongly affected by the viscosity and the size of the damping orifice. So it was very necessary to figure out the vibration characteristics of the pneumatic PVEH. On the other hand, it could be seen from the working principle that the flow of the compressed air mainly depended on the damping orifice and the proof mass, meanwhile, the bending strain of the piezoelectric diaphragm was totally decided by the pressure difference. In addition, the various pressures of the compressed air before working would lead to the different initial working conditions of the pneumatic PVEH. So the effects of the dimension of the damping orifice, initial air pressure and proof mass on the power generation characteristics needed to be explored. Nevertheless, because the proposed PVEH was a fairly complicated coupled system with both the air-solid and mechanical-electrical interactions, it was very difficult to build an accurate mathematical model. This work would mainly focus on the experimental investigation of the pneumatic PVEH. We also expected that some key rules could be found from experiments to further establish a set of theoretical system to characterize the pneumatic PVEH.

## 2. Fabrication and experiments

In view of the above facts, a prototype of the pneumatic PVEH with one piezoelectric transducer was fabricated and tested to verify the principle as well as estimate the performance. The piezoelectric transducer was composed of a piezoelectric disk, top & bottom covers and O-ring, where two symmetrical cavities were formed between the piezoelectric disk and shells. A commercial unimorph piezoelectric disk was adopted, where the piezoelectric material was PZT-4 element with the size of $\Theta 60 \times 0.2$ mm$^3$ and the brass was used for the disk substrate with the size of $\Theta 65 \times 0.4$ mm$^3$. The transducer shells were made of polymethyl methacrylate (PMMA) with the advantages of easy processing, light weight, insulation and easy observation as well as the shell was fabricated by CNC engraving and milling machine.

A double-acting single-rod piston cylinder with the inner diameter of $\Theta 16$ mm and the body length of 200 mm was utilized to bear the weight of the proof mass. To ensure the stability of the vibrating proof mass, three parallel balance springs with the same length and stiffness

as well as three corresponding guide rods were applied in the experiment. The plastic tubes were used to connect the cylinder and the piezoelectric transducer. The cylinder was mounted on a shaker (DC-1000, Sushi) from Sushi Testing Instruments co., Ltd of China. It could achieve a maximum acceleration of 980 m/s$^2$, a maximum displacement of 51 mm, and a maximum velocity of 2.0 m/s with a frequency range of 5–3500 Hz. The sinusoidal excitation signal with the vibration amplitude of 1 mm and the initial phase of 0° was generated using a digital sinusoidal/random vibration control system (RC-3000-4, Sushi) and amplified by a switching power amplifier including an excitation power (SA-15, Sushi). One single-axis piezoelectric accelerometer (2106C, Sushi) was utilized to form the closed-loop control of the shaker and the other one was employed to measure the vibrational displacement of the proof mass according to the relationship between the acceleration $a$, frequency $f$, and the amplitude $A$ (half of the displacement), i.e., $a = A(2\pi f)^2$ [59]. The main parameters of the piezoelectric accelerometers were as follows: a sensitivity of 50 mV/g ($\pm 5\%$), a measurement range of 100 g, a frequency range of 1–5000 Hz ($\pm 10\%$), a linearity of $< 1\%$, and the output impedance of $< 100$ Ω. A digital oscilloscope (GDS-1102, GW Instek) was used to measure the peak-to-peak open-circuit voltage and its accuracy was $\pm 3\%$. A digital pressure gage (DIM 20, Afriso) was used to display the system pressure, with the measurement range of 40 MPa and the accuracy of $\pm 1\%$ FSO. The dumbbell discs with the accuracy of ~5% were used as the proof mass because there were not heavy standard weights in our laboratory. A cut-off valve was exploited to serve as the damping orifice, where the size of the damping orifice could be altered through adjusting the opening degree of the valve. It should be noted that the opening degree was set by default in full-open mode unless the effect of the damping orifice on the performance was investigated. The assembled piezoelectric transducer and the experimental setup are presented in Fig. 2. In this setup, both the vibrational displacement and the open-circuit voltage versus frequency characteristics under different proof mass, air pressure and damping orifice were tested to validate the feasibility of the proposed principle as well as figure out the performance of the pneumatic PVEH.

## 3. Results

### 3.1. Frequency responses of vibrational displacement output

In this section, to explore the vibration characteristics of the pneumatic PVEH and investigate how its performance was affected by the proof mass, air pressure and damping orifice, corresponding
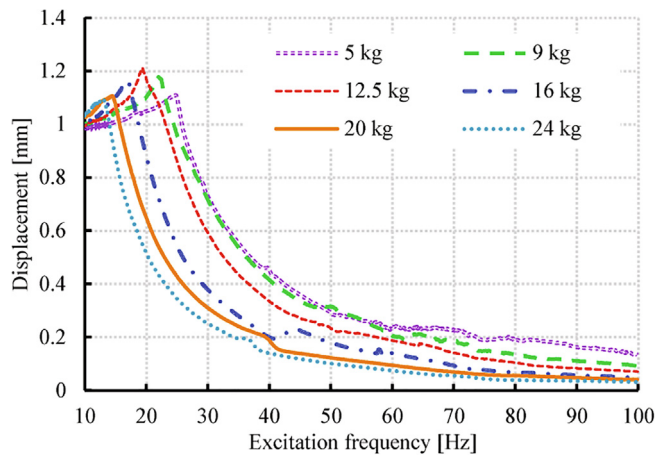
**Fig. 3.** The vibrational displacement-frequency responses of the pneumatic PVEH under different proof masses with an air pressure of 0.7 MPa.



**Fig. 4.** The vibrational displacement-frequency responses of the pneumatic PVEH under different air pressures with the proof mass of 9 kg.

**Table 2**
Peak displacement and peak frequency under different air pressures.

| Air pressure (MPa) | Peak displacement (mm) | Optimal frequency (Hz) |
| --- | --- | --- |
| 0.1 | 1.16 | 20.77 |
| 0.3 | 1.17 | 20.46 |
| 0.5 | 1.20 | 21.33 |
| 0.6 | 1.20 | 20.77 |
| 0.75 | 1.21 | 21.43 |
| 0.95 | 1.23 | 21.29 |

experiments were designed and carried out. Next, the influence of these three factors on the frequency-dependent vibrational displacement was demonstrated by experiments, respectively. It should be noted that the displacement was transformed from the acceleration under the frequency sweeping mode, where a sweep rate of 0.15 Hz/s was set. Such a frequency-sweeping method was widely applied in vibration testing and energy harvesting [60].

Fig. 3 shows a sweep of the vibrational displacement versus excitation frequency under different proof masses with an air pressure of 0.7 MPa for the pneumatic PVEH. The experimental results demonstrated that the vibrational displacement was greater than the excitation amplitude in low frequency band (about < 30 Hz) no matter what proof mass. Yet, the displacement presented a trend of approaching zero rapidly in high frequency band (about > 50 Hz). In another word, there was an optimal excitation frequency where the vibrational displacement reached the peak value for each measured proof mass. Furthermore, it was observed that when the proof mass was increased to 12.5 kg, the PVEH achieved a maximum displacement of 1.21 mm at 19.34 Hz. Besides, it was noticed that the optimal frequency decreased with the enhancement of the proof mass. It was in accordance with the rule that the resonance frequency decreased with the increasing mass. The measured peak displacement and its corresponding excitation frequency under different proof masses are listed in Table 1. The detailed experimental data were as follows. The peak displacements of 1.11 mm, 1.18 mm, 1.21 mm, 1.16 mm, 1.10 mm, and 1.09 mm were recorded at 24.73 Hz, 21.94 Hz, 19.34 Hz, 16.90 Hz, 14.43 Hz, and 13.04 Hz for the PVEH under the proof masses of 5 kg, 9 kg, 12.5 kg, 16 kg, 20 kg, and 24 kg, respectively.

Fig. 4 illustrates displacement-frequency responses under different initial air pressures with a proof mass of 9 kg for the pneumatic PVEH. Compared with the influence of the proof mass on the vibration characteristics, the PVEH shows a fairly similar trend of the vibrational displacement with the air pressure except that the peak displacement demonstrates an increasing trend with the rising air pressure, as shown in Fig. 4. The measured peak displacement and its corresponding

frequency under different air pressures are listed in Table 2. The maximum displacement of 1.23 mm was observed at 21.29 Hz with the proof mass of 9 kg when the air pressure was increased to 0.95 MPa. For other measured pressures, the peak displacements of 1.16 mm, 1.17 mm, 1.20 mm, 1.20 mm, and 1.21 mm were achieved at 20.77 Hz, 20.46 Hz, 21.33 Hz, 20.77 Hz, and 21.43 Hz for the pneumatic PVEH under the air pressures of 0.1 MPa, 0.3 MPa, 0.5 MPa, 0.6 MPa, and 0.75 MPa, respectively. Experimental results showed that a larger vibrational displacement could be achieved by enhancing the air pressure. Furthermore, the optimal frequency of the vibrational displacement was hardly affected by the air pressure. The optimal frequency only presented the fluctuation of < 1 Hz on the vibrational displacement-frequency response curves with the increasing air pressure from 0.1 MPa to 0.95 MPa.

Fig. 5 depicts a sweep of the vibrational displacement versus excitation frequency under different dimensions of the damping orifice with a 9-kg proof mass and 0.5-MPa air pressure for the pneumatic PVEH. As mentioned above, because it was very difficult to obtain the accurate orifice size, the different opening degrees of the cut-off valve were used to approximately represent the dimension change of the damping orifice. As shown in Fig. 5, four displacement-frequency response curves with different damping orifices present a roughly similar trend. Moreover, the damping orifice brings a quite similar influence on both the peak displacement and the optimal excitation frequency. With the increasing size of the damping orifice, both the peak displacement and the optimal frequency were firstly enhanced and then decreased. The measured peak displacement and the corresponding excitation frequency under different valve opening are listed in Table 3. When the opening degree of the valve was around the half, the vibrational displacement reached a maximum value of 1.22 mm at the frequency of 22.42 Hz. For other opening degree, the peak displacements of 1.17 mm, 1.20 mm, and 1.20 mm were recorded at 20.32 Hz, 21.87 Hz, and 21.33 Hz for the pneumatic PVEH under the valve opening of 1/6, 1/3, and 100%, respectively.

**Table 1**
Peak displacement and peak frequency under different proof masses.

| Proof mass (kg) | Peak displacement (mm) | Optimal frequency (Hz) |
| --- | --- | --- |
| 5 | 1.11 | 24.73 |
| 9 | 1.18 | 21.94 |
| 12.5 | 1.21 | 19.34 |
| 16 | 1.16 | 16.90 |
| 20 | 1.10 | 14.43 |
| 24 | 1.09 | 13.04 |
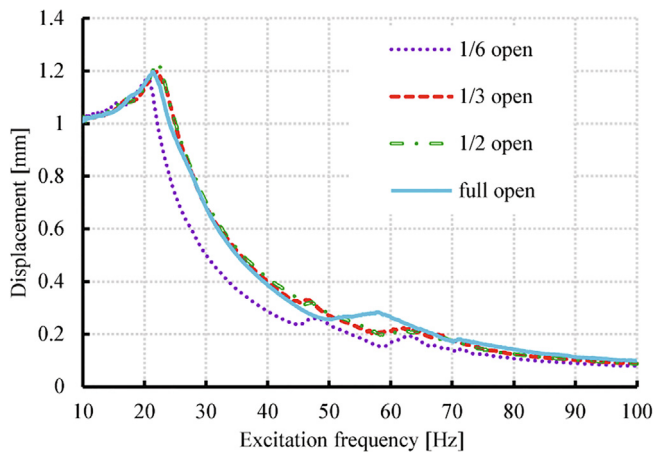
**Fig. 5.** The vibrational displacement-frequency responses of the pneumatic PVEH under different damping orifices with a 9-kg proof mass and 0.5-MPa air pressure.

**Table 3**
Peak displacement and peak frequency under different valve opening.

| Valve opening | Peak displacement (mm) | Optimal frequency (Hz) |
|---|---|---|
| 1/6 | 1.17 | 20.32 |
| 1/3 | 1.20 | 21.87 |
| 1/2 | 1.22 | 22.42 |
| 100% | 1.20 | 21.33 |

### 3.2. Frequency responses of open-circuit voltage output

Through the experiments above, there has been a general overview of the vibration characteristics for the pneumatic PVEH. Nevertheless, it was no doubt that the power generation performance was more important for energy harvesters. Next, the effects of above-mentioned factors, namely proof mass, air pressure and damping orifice, on the power generation characteristics were further tested and analyzed. Because the shaker provided a sinusoidal base excitation to the mounted pneumatic PVEH in the experiments, the output voltage generated by the piezoelectric element was also a sine wave. Like some other literatures, the peak-to-peak voltage was directly recorded through the digital oscilloscope, namely the peak-to-peak open-circuit voltage. Fig. 6 presents the relationship between the peak-to-peak open-circuit voltage and the excitation frequency under different masses with
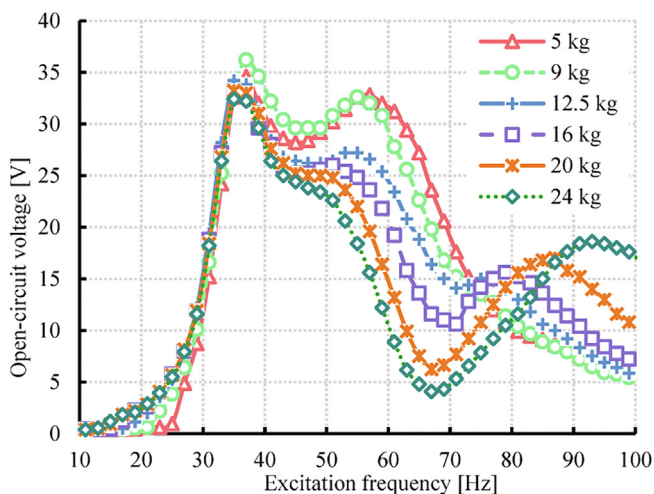
**Table 4**
Peak voltage output and peak frequency under different proof masses.

| Proof mass (kg) | Peak voltage (V) | Optimal frequency (Hz) |
|---|---|---|
| 5 | 34.6 | 37 |
| 9 | 36.2 | 37 |
| 12.5 | 34.2 | 35 |
| 16 | 33.2 | 35 |
| 20 | 33.2 | 35 |
| 24 | 32.4 | 35 |

an air pressure of 0.7 MPa. The experimental results showed that there existed two obvious resonance peaks in the frequency range of 10–100 Hz no matter what proof mass was loaded as well as the first peak voltage was greater than the second one. There was an optimal proof mass to maximize the output voltage. The measured peak voltage and its corresponding frequency under different proof masses are listed in Table 4. When the proof mass was equal to 9 kg, the maximum peak-to-peak open-circuit voltage of 36.2 V was achieved at 37 Hz. However, it was found that the proof mass did not introduce much effect on the optimal excitation frequency (namely the first resonance frequency) after the vibration of the proof mass was transferred via the compressed air, compared with the effect of proof mass on vibration characteristics. When the proof mass was increased from 5 kg to 24 kg, the optimal excitation frequency decreased from 37 Hz to 35 Hz, i.e., only a fluctuation of 2 Hz. The optimal frequency of 35 Hz was even kept constant as the mass varied from 12.5 kg to 24 kg. Furthermore, the second resonance frequency was increased with the enhancing proof mass. The specific experimental data were as follows. The peak voltages of 34.6 V, 36.2 V, 34.2 V, 33.2 V, 33.2 V, and 32.4 V were recorded at 37 Hz, 37 Hz, 35 Hz, 35 Hz, 35 Hz, and 35 Hz for the PVEH under the proof masses of 5 kg, 9 kg, 12.5 kg, 16 kg, 20 kg, and 24 kg, respectively.

Fig. 7 depicts the relationship between the air pressure and the peak-to-peak open-circuit voltage with the proof mass of 9 kg in the excitation frequency range of 10–100 Hz. It was observed from Fig. 7 that there was only one peak in the voltage-frequency curves when the initial air pressure was less than 0.5 MPa, whereas two peaks were displayed at the pressure of more than 0.5 MPa. The peak voltage firstly increased and then basically remained unchanged with the rising air pressure. However, the optimal frequency of voltage-frequency response curves dropped almost linearly with the increasing air pressure. In the experiment, when the air pressure was changed from 0.1 MPa to 0.95 MPa, the optimal excitation frequency decreased from 55 Hz to 31 Hz. The measured peak voltage and its corresponding frequency under different air pressures are listed in Table 5. The specific recorded



**Fig. 6.** The output voltage-frequency responses of the pneumatic PVEH under different proof masses with an air pressure of 0.7 MPa.
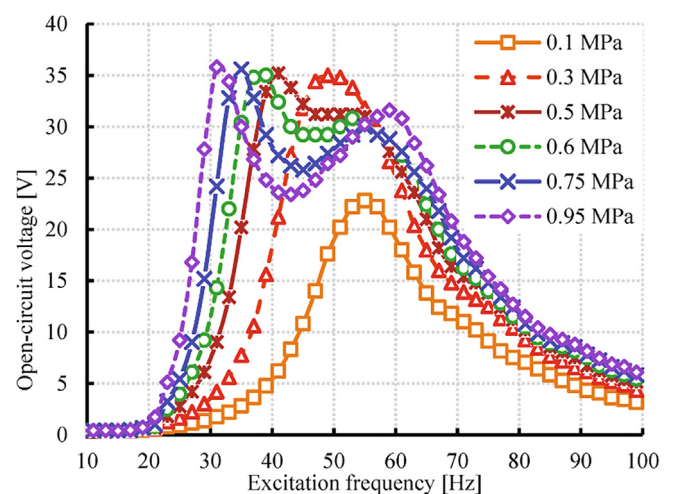


**Fig. 7.** The output voltage-frequency responses of the pneumatic PVEH under different air pressures with the proof mass of 9 kg.

**Table 5**
Peak voltage output and peak frequency under different air pressures.

| Air pressure (MPa) | Peak voltage (V) | Optimal frequency (Hz) |
|---|---|---|
| 0.1 | 22.8 | 55 |
| 0.3 | 35 | 49 |
| 0.5 | 35.2 | 41 |
| 0.6 | 35 | 39 |
| 0.75 | 35.6 | 35 |
| 0.95 | 35.8 | 31 |

**Table 6**
Peak voltage output and peak frequency under different valve opening.

| Valve opening | Peak voltage (V) | Optimal frequency (Hz) |
|---|---|---|
| 1/6 | 51.6 | 55 |
| 1/3 | 39.2 | 55 |
| 1/2 | 35.2 | 41 |
| 100% | 35.2 | 41 |

experimental data were as follows. The peak voltages of 22.8 V, 35 V, 35.2 V, 35 V, 35.6 V, and 35.8 V were achieved at 55 Hz, 49 Hz, 41 Hz, 39 Hz, 35 Hz, and 31 Hz for the PVEH under the air pressures of 0.1 MPa, 0.3 MPa, 0.5 MPa, 0.6 MPa, 0.75 MPa, and 0.95 MPa, respectively. Because the volume of the cylinder chambers was basically fixed without considering the elastic deformation of plastic tubes, the increase of the air pressure actually added the amount of the air. It meant that the mass was enhanced and the optimal excitation frequency was thus decreased. In addition, both the second peak voltage and its resonance frequency had an increasing trend as the air pressure rose, i.e., the distance between two peak voltages increased with the rising air pressure.

The compressed air was able to flow through a damping orifice because of the pressure difference. As we know, the air movement and pressure loss are tightly associated with the flow area of the orifice. So, it could be inferred that the orifice diameter brought a strong influence on the power generation characteristics of the pneumatic PVEH. Fig. 8 presents the generated voltage-frequency responses under different damping orifices with a 9-kg proof mass and 0.5-MPa air pressure. As shown in Fig. 8, the peak number of the voltage-frequency response curves demonstrates a trend of transition from 1 to 2 as the orifice size increases. The open-circuit voltage decreased with the increasing orifice size until the opening degree of valve was the half. Apparently, the pressure loss would increase with the decreasing flow area of the orifice. In other words, the pressure difference decreases with the increasing orifice diameter. Therefore, the open-circuit voltage was also decreased with the enhancing orifice size because the output voltage was in proportion to the pressure difference. Besides, when the opening degree of the cut-off valve was adjusted to 1/6, a maximum peak-to-peak voltage of 51.6 V was observed at 55 Hz and 0.5-MPa air pressure for this PVEH. Nevertheless, the voltage-frequency response curves are quite similar when the opening degree is greater than 1/2, as depicted in Fig. 8. It meant that the pressure difference between the both sides of the piezoelectric diaphragm would remain unchanged as the orifice
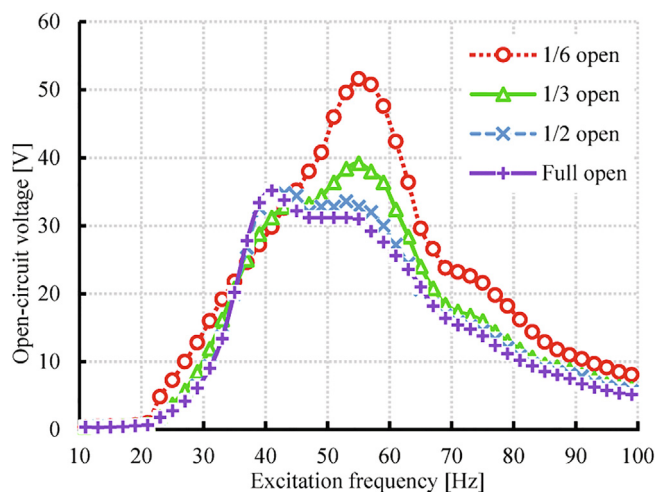


**Fig. 8.** The output voltage-frequency responses of the pneumatic PVEH under different damping orifices with a 9-kg proof mass and 0.5-MPa air pressure.

diameter increased to a certain degree. As for the optimal frequency, it was roughly decreased with the rising orifice size. Nevertheless, there were the same optimal frequencies for the single-peak curves, and the 2-peak curves as well. The measured peak voltage and its corresponding excitation frequency under different valve opening are listed in Table 6. Specifically, the peak voltages of 51.6 V, 39.2 V, 35.2 V, and 35.2 V were recorded at 55 Hz, 55 Hz, 41 Hz, and 41 Hz for the pneumatic PVEH under the valve opening of 1/6, 1/3, 1/2, and 100%, respectively.

## 4. Discussion

By making use of the pressure energy rather than kinetic energy of the air, a novel pneumatic PVEH based on the compressed air-transducer-structure interaction was proposed and the feasibility of the novel PVEH was proved by the experiments in this study. Unlike previous most PVEHs where the piezoelectric elements were directly subjected to the vibration, the energy conversion was performed in the pneumatic PVEH twice, namely the kinetic energy → pressure energy → electric energy. So, the PVEH performance in terms of vibrational displacement and peak-to-peak open-circuit voltage was experimentally investigated, respectively. Experimental results showed that the proof mass, initial air pressure and damping orifice exerted a strong impact on the vibration and power generation characteristics for the pneumatic PVEH.

### 4.1. Influence factor analysis of energy harvesting performance

To verify the principle of the proposed PVEH, the energy harvesting performance of the fabricated PVEH prototype was experimentally characterized. Among three influencing factors, the proof mass had very little effect on both the optimal frequency point and the corresponding output voltage. However, the proof mass brought a significant influence on another important property of the energy harvester, namely the frequency bandwidth. If an output voltage of 20 V was randomly adopted as the criterion of the working bandwidth, the response ranges around the resonance frequency of the pneumatic PVEH were approximately 37 Hz, 35 Hz, 31 Hz, 29 Hz, 25 Hz, and 21 Hz with the proof mass of 5 kg, 9 kg, 12.5 kg, 16 kg, 20 kg, and 24 kg, respectively. It meant that the working bandwidth was steadily decreased with the increasing proof mass. Note that it only took 20 V as an example and there would exist a consistent trend if other voltage criteria were used to show the influence of proof mass on the working bandwidth.

It was via the transfer medium of the compressed air that the PVEH converted the vibration energy into electrical energy. So it could be inferred that the effect of the air pressure on the energy harvesting performance would be more complex than that of the proof mass. The voltage-frequency response curves with different air pressures showed that the optimal frequency as well as the maximum output voltage was strongly changed with the air pressure. What's more, the pressure also had a strong influence on the frequency bandwidth of the PVEH. The reference voltage of 20 V was still used to characterize the working bandwidth. The response ranges around the resonance frequency were as follows: 8 Hz at 0.1 MPa, 23 Hz at 0.3 MPa, 30 Hz at 0.5 MPa, 35 Hz at 0.6 MPa, 39 Hz at 0.75 MPa, and 41 Hz at 0.95 MPa. It showed that

the working bandwidth was significantly increased with the increasing air pressure. The bandwidth of the PVEH at 0.95 MPa was five times wider than that of the PVEH at 0.1 MPa. Apart from the above influence, the PVEH was changed from single-degree-of-freedom (single DOF) vibration system to 2-DOF system with the rising air pressure. The possible reason was that the equivalent stiffness of the compressed air increased with the increasing pressure. Anyway, the 2-DOF system brought an apparent benefit in terms of bandwidth for the pneumatic PVEH. The analysis results showed that high air pressure was helpful to enhance the generated voltage as well as broaden the useful bandwidth. However, if an excessive pressure was employed in the experiments, a heavy load would also be exerted on the piezoelectric transducer, which might lead to the damage of the piezoelectric element due to the too large pressure difference. Furthermore, in view of the sealing of the piston-cylinder system and piezoelectric transducer, it was not suitable to adopt an excessive pressure, either. So the air pressure applied in the experiments was less than 1 MPa.

Because the damping orifice had a great impact on the air mobility as well as the pressure difference, we could reasonably predict that it was also a complicated influencing factor for the PVEH. Actually, it can be seen from Fig. 8 that the effect of the damping orifice was similar to that of the air pressure, the maximum output voltage, optimal frequency, frequency bandwidth and peak number were strongly affected by the orifice. Similarly, when the reference voltage of 20 V was also exploited to estimate the bandwidth, the response ranges around the resonance frequency were about 42 Hz with 1/6 open, 33 Hz with 1/3 open, 31 Hz with 1/2 open, and 31 Hz with full open, respectively. It indicated that the working bandwidth increased with the decreasing orifice size. Also, the PVEH presented the property of a single-DOF system when the opening degree was less than 1/3, whereas it became a 2-DOF system as the opening degree increased to 1/2. The reason why the damping orifice influenced the degree of freedom of the pneumatic PVEH needs to be further explored in future. The analysis results showed that a small damping orifice was beneficial for energy harvesting to produce large voltage output and broaden frequency bandwidth. It was noticed that the maximum voltage increased drastically with the reducing orifice size. Undoubtedly, the higher voltage output meant that a larger deformation of piezoelectric element was required. As we know, most of the piezoelectric elements used in the PVEHs are PZT materials which are easily breakable with large deformation. So the reliability of the pneumatic PVEH would be reduced with the decreasing orifice.

### 4.2. Comparison between the vibration and power generation characteristics

Firstly, the effects of the proof mass on vibration behaviors and power generation characteristics were compared and analyzed. The maximum vibrational displacement, the maximum open-circuit voltage and their corresponding optimal frequencies were extracted from Figs. 3 and 6, respectively. Then the comparison of effects of the proof mass can be further presented, as depicted in Fig. 9. The comparison results indicated that the optimal proof masses maximizing the displacement and voltage were different, where the proof masses were 12.5 kg and 9 kg, respectively. On the other hand, the effect of the proof mass on their corresponding optimal frequency was totally different as well. The optimal frequency of the vibrational displacement was much smaller than that of the output voltage under the same proof mass. Furthermore, the optimal frequency was significantly deceased with the increasing proof mass for the vibration properties, whereas the optimal frequency presented a very modest change with the proof mass for the power generation properties. Generally, for the existing PVEHs, when some a proof mass maximized the vibrational displacement, the output voltage would also reach the maximum under this proof mass. Moreover, their corresponding maximum values basically occurred at the same optimal frequencies. That is, the vibration characteristics were consistent with the power generation characteristics. In contrast, it was

found that the proof mass led to a completely different influence on the vibration and power generation performance for the pneumatic PVEH.

Secondly, by extracting the maximum vibrational displacement and open-circuit voltage as well as their corresponding optimal frequencies from Figs. 4 and 7, a comparison of effects of the air pressure on vibration characteristics and power generation characteristics is given in Fig. 10. The comparison results showed that the influence of the air pressure on the vibration behaviors and power generation characteristics was also different. In general, the air pressure brought a larger influence on the power generation performance than on the vibration characteristics. The peak number of the voltage increased from 1 to 2 with the rising air pressure, whereas there was only one peak displacement in the range from 10 Hz to 100 Hz. In terms of the displacement and voltage, the maximum vibrational displacement was significantly increased with the increasing air pressure. In contrast, though the maximum open-circuit voltage also increased firstly, yet it would basically be kept unchanged when the air pressure was greater than 0.3 MPa in this work. As for the optimal frequency, the optimal frequency of vibrational displacement was much smaller than that of output voltage under the same air pressure. Nevertheless, the air pressure brought a quite opposite impact on the vibration behaviors and power generation characteristics, compared with the influence of the proof mass on them. As mentioned above, the proof mass had a very small influence on the optimal frequency of the output voltage. By comparison, the air pressure hardly affected the optimal frequency of the displacement. However, the optimal frequency of the voltage-frequency response curves was almost linearly decreased with the enhancing air pressure, where it was similar to the influence of the proof mass on the displacement.

Thirdly, by means of the similar method, the comparison of effects of the damping orifice can be presented through extracting Figs. 5 and 8, as illustrated in Fig. 11. The comparison results showed the damping orifice also brought a completely different impact on the vibration and power generation characteristics. In terms of the peak number, the influence of the damping orifice was a bit similar to that of the air pressure. Although only one peak displacement was observed no matter what the opening degree of the valve was, it seemed there was a threshold value of the orifice size to alter the peak number for the voltage characteristics. When the opening degree of the cut-off valve exceeded 1/2, the peak number of output voltage was changed from 1 to 2 in this study. In comparison to the trend of the maximum vibrational displacement and open-circuit voltage with the excitation frequency, there was an optimal orifice size to maximize vibrational displacement. However, the maximum output voltage decreased first and then remained unchanged with the increasing orifice size. For the optimal frequency, the above-mentioned influence of the orifice size on the maximum displacement and voltage could be applicable for the effect on the optimal frequency as well. But the optimal frequency of output voltage was much greater than that of vibrational displacement under the same orifice size.

A direct comparison indicated that the effects of proof mass, air pressure and damping orifice on the vibration characteristics differed from the one on the power generation characteristics for the pneumatic PVEH. It could be regarded as one of differences between the previous most PVEHs and the novel PVEH. In another word, a PVEH independent of the vibration properties could be constructed. For example, we could obtain a kind of PVEH where the optimal frequency of output voltage was barely changed with the additional proof mass. At the same time, an effective approach was provided to achieve a desired performance, namely adjusting the proof mass, air pressure and damping orifice. For instance, the frequency bandwidth of the pneumatic PVEH could be broadened through enhancing the initial air pressure to produce more voltage peaks, the output voltage could be enhanced through decreasing the size of damping orifice. In addition, because the deformation of the piezoelectric element was directly caused by the pressure difference of the compressed air rather than the proof mass,
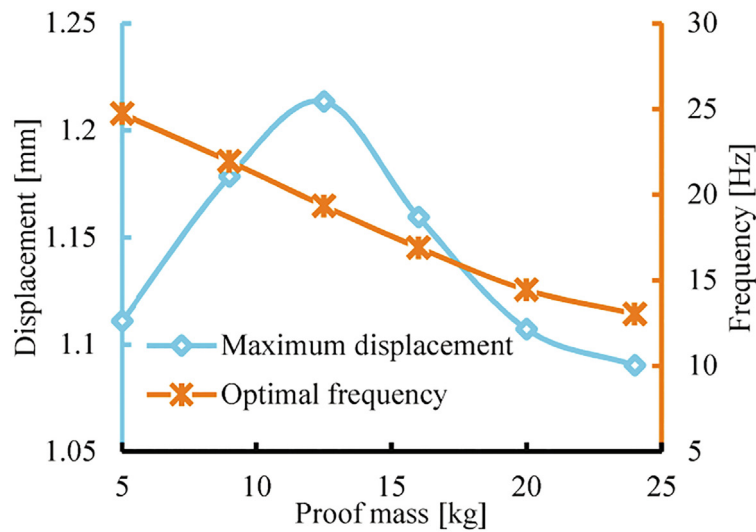
(a) Effects of the proof mass on vibration characteristics.
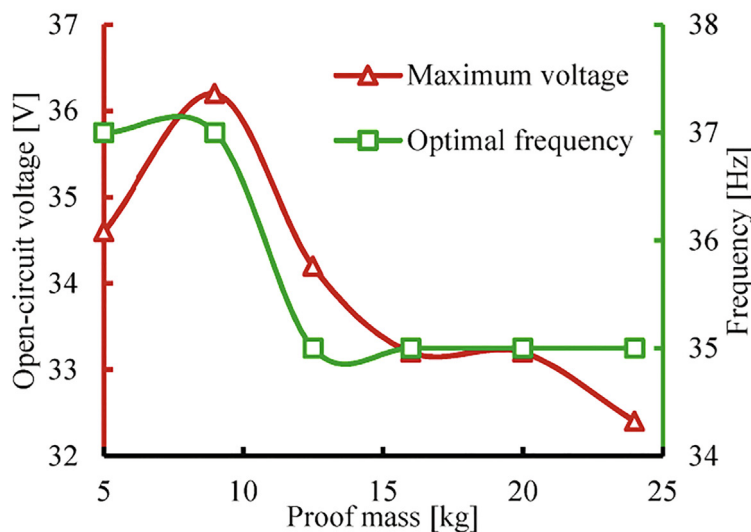


(b) Effects of the proof mass on power generation characteristics.

**Fig. 9.** Comparison of effects of the proof mass on vibration characteristics and power generation characteristics of the pneumatic PVEH.

the proposed PVEH could tolerate a heavier load compared with the classical PVEH. Moreover, the pressure difference could be further adjusted by the damping orifice. Relatively speaking, the proposed PVEH could have a higher reliability and durability than the most classical PVEHs under the same heavy loads. The high reliability was also mainly one of advantages of the pneumatic PVEH. It is noted that this paper only takes PZT as an example to validate the feasibility of the presented PVEH, other piezoelectric materials like piezoelectric polymers, piezoelectric thin film and MFC can also be used to construct the pneumatic PVEH. Moreover, because the pneumatic PVEH realizes the energy conversion and motion transmission through the air medium, the electricity-generating capacity can easily be improved by using multiple piezoelectric transducers. Presently, pneumatic transmission systems powered by the compressed air are widely used in industrial production automation due to the advantages of convenient and green sources,

good adaptability to the environment, easy implementation of auto control and long-distance transportation. Meanwhile, pneumatic technology plays an increasingly important role in vibration isolation and suppression. Various pneumatic devices are constantly emerging, such as pneumatic shock absorbers, pneumatic isolators and pneumatic dampers. In these circumstances, if the vibration energy is harvested to generate enough electric energy, the semi-active structural vibration control can be further realized.

## 5. Conclusions

A novel pneumatic piezoelectric vibration energy harvester (PVEH) based on the compressed air-transducer-structure interaction is proposed in this paper. The pneumatic PVEH firstly converted the kinetic energy of the vibration into the pressure energy of the air and then the
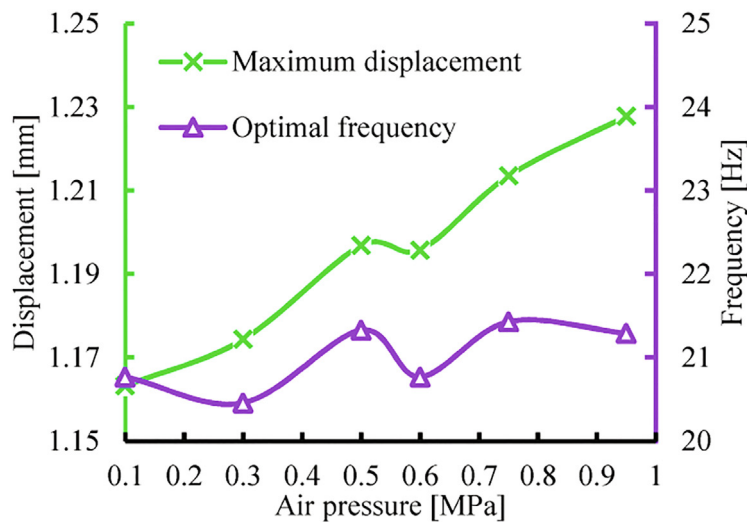
(a) Effects of the air pressure on vibration characteristics.
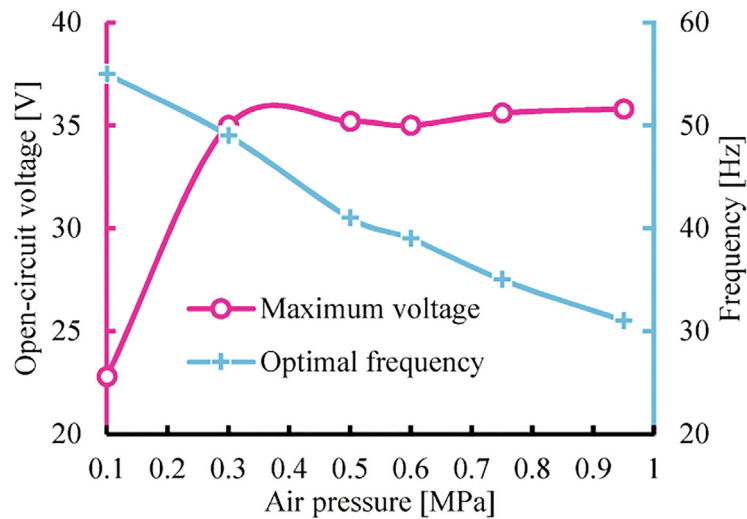


(b) Effects of the air pressure on power generation characteristics.

**Fig. 10.** Comparison of effects of the air pressure on vibration characteristics and power generation characteristics of the pneumatic PVEH.

pressure difference caused by the damping orifice forced the piezoelectric transducer to generate the electric energy. To verify the feasibility of the pneumatic PVEH, a prototype was fabricated and the test of frequency characteristics was carried out by experiments. The results showed that the initial air pressure, proof mass and damping orifice brought a significant influence on the vibration and power generation properties for the pneumatic PVEH. Moreover, it was found that the influence of the proof mass, air pressure and damping orifice on the vibration characteristics was totally different from that of the power generation characteristics. No matter how the above factors changed, there was only one peak displacement within the frequency range of 10–100 Hz in terms of the vibration properties. By contrast, more than one peak voltage would occur with the increase of the air pressure or the size of the damping orifice for the power generation characteristics. The optimal frequency of output voltage was much greater than that of vibrational displacement. So one of the important features of the pneumatic PVEH was that power generation characteristics were not limited by the vibration behaviors. In addition, the experimental results

indicated that there was an optimal proof mass to maximize the open-circuit voltage of the pneumatic PVEH. The optimal frequency of the output voltage decreased linearly with the rising air pressure. When the air pressure was increased from 0.1 MPa to 0.95 MPa, the optimal excitation frequency decreased from 55 Hz to 31 Hz. The open-circuit voltage could be improved through decreasing the size of damping orifice, where the output voltage reached the maximum value of 51.6 V at the air pressure of 0.5 MPa with the valve opening of 1/6 for the pneumatic PVEH.

**CRediT authorship contribution statement**

**Zhonghua Zhang:** Conceptualization, Investigation, Writing - original draft. **Shuyun Wang:** Supervision, Writing - review & editing. **Junwu Kan:** Investigation, Writing - review & editing, Formal analysis. **Wenjing Hu:** Visualization, Data curation. **Zefeng Chen:** Validation, Visualization. **Hailong Xu:** Investigation, Validation.
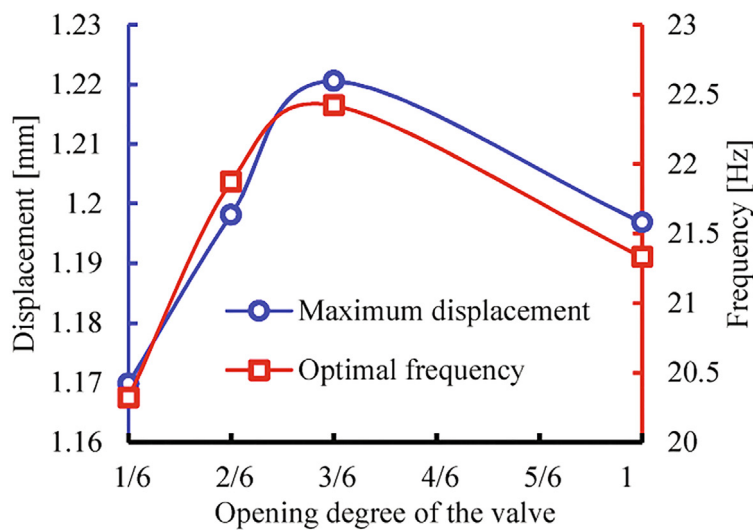
(a) Effects of the orifice size on vibration characteristics.
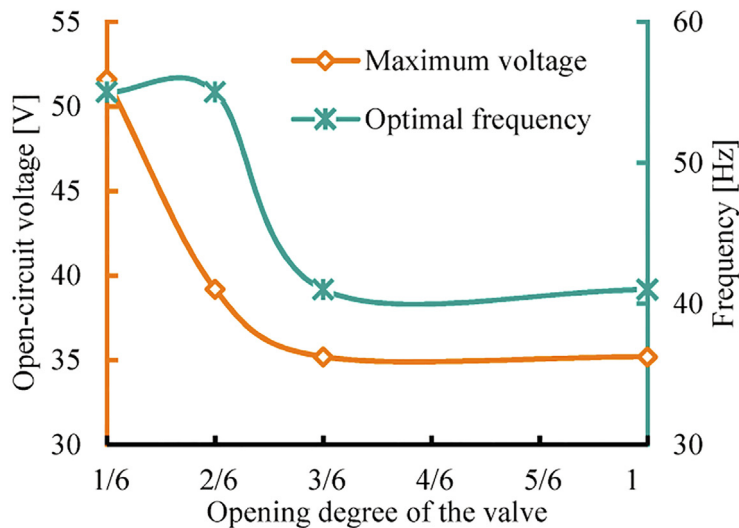


(b) Effects of the orifice size on power generation characteristics.

**Fig. 11.** Comparison of effects of the orifice size on vibration characteristics and power generation characteristics of the pneumatic PVEH.

## Declaration of Competing Interest

The authors declare that they have no known competing financial interests or personal relationships that could have appeared to influence the work reported in this paper.

## References

[1] Amini Y, Heshmati M, Fatehi P, Habibi SE. Piezoelectric energy harvesting from vibrations of a beam subjected to multi-moving loads. Appl Math Model 2017;49:1–16.

[2] Wei CF, Jing XJ. A comprehensive review on vibration energy harvesting: modelling and realization. Renew Sustain Energy Rev 2017;74:1–18.

[3] Kan JW, Fu JW, Wang SY, Zhang ZH, Chen S, Yang C. Study on a piezo-disk energy harvester excited by rotary magnets. Energy 2017;122:62–9.

[4] Hales A, Jiang X. A review of piezoelectric fans for low energy cooling of power electronics. Appl Energy 2018;215:321–37.

[5] Siddique AM, Mahmud S, Van Heyst B. A comprehensive review on vibration based micro power generators using electromagnetic and piezoelectric transducer mechanisms. Energy Convers Manage 2015;106:728–47.

[6] Toyabur RM, Salauddin M, Cho H, Park JY. A multimodal hybrid energy harvester based on piezoelectric-electromagnetic mechanisms for low-frequency ambient vibrations. Energy Convers Manage 2018;168:454–66.

[7] Zhang X, Pan H, Qi L, Zhang Z, Yuan Y, Liu Y. A renewable energy harvesting system using a mechanical vibration rectifier (MVR) for railroads. Appl Energy 2017;204:1535–43.

[8] Abdelmoula H, Sharpes N, Abdelkefi A, Lee H, Priya S. Low-frequency Zigzag energy harvesters operating in torsion-dominant mode. Appl Energy 2017;204:413–9.

[9] Ilyas MA, Swingler J. Piezoelectric energy harvesting from raindrop impacts. Energy 2015;90:796–806.

[10] Khalatkar AM, Gupta VK. Piezoelectric energy harvester for low engine vibrations. J

Renewable Sustainable Energy 2017;9:024701.

[11] Erturk A, Inman DJ. On mechanical modeling of cantilevered piezoelectric vibration energy harvesters. J Intell Mater Syst Struct 2008;19:1311–25.

[12] Cheng T, Fu X, Liu W, Lu X, Chen X, Wang Y, et al. Airfoil-based cantilevered polyvinylidene fluoride layer generator for translating amplified air-flow energy. Renewable Energy 2019;135:399–407.

[13] Bai Y, Tofel P, Hadas Z, Smilek J, Losak P, Skarvada P, et al. Investigation of a cantilever structured piezoelectric energy harvester used for wearable devices with random vibration input. Mech Syst Sig Process 2018;106:303–18.

[14] Zhang ZH, Kan JW, Wang SY, Wang HY, Yang C, Chen S. Performance dependence on initial free-end levitation of a magnetically levitated piezoelectric vibration energy harvester with a composite cantilever beam. IEEE Access 2017;5:27563–72.

[15] Wang W, Huang RJ, Huang CJ, Li LF. Energy harvester array using piezoelectric circular diaphragm for rail vibration. Acta Mech Sin 2014;30:884–8.

[16] Xiao Z, Yang TQ, Dong Y, Wang XC. Energy harvester array using piezoelectric circular diaphragm for broadband vibration. Appl Phys Lett 2014;104:223904.

[17] Yang Y, Li Y, Guo Y, Xu BX, Yang T. Improved vibration-based energy harvesting by annular mass configuration of piezoelectric circular diaphragms. Smart Mater Struct 2018;27:035004.

[18] Feenstra J, Granstrom J, Sodano H. Energy harvesting through a backpack employing a mechanically amplified piezoelectric stack. Mech Syst Signal Process 2008;22:721–34.

[19] Wang C, Wang S, Li QJ, Wang X, Gao Z, Zhang L. Fabrication and performance of a power generation device based on stacked piezoelectric energy-harvesting units for pavements. Energy Convers Manage 2018;163:196–207.

[20] Daniliuk V, Xu Y, Liu R, He T, Wang X. Ultrasonic de-icing of wind turbine blades: performance comparison of perspective transducers. Renewable Energy 2020;145:2005–18.

[21] Palosaari J, Leinonen M, Hannu J, Juuti J, Jantunen H. Energy harvesting with a cymbal type piezoelectric transducer from low frequency compression. J Electroceram 2012;28:214–9.

[22] Li X, Guo M, Dong S. A flex-compressive-mode piezoelectric transducer for mechanical vibration/strain energy harvesting. IEEE Trans Ultrason Ferroelectr Freq Control 2011;58:698–703.

[23] Moure A, Rodríguez MI, Rueda SH, Gonzalo A, Rubio-Marcos F, Cuadros DU, et al. Feasible integration in asphalt of piezoelectric cymbals for vibration energy harvesting. Energy Convers Manage 2016;112:246–53.

[24] Jasim A, Wang H, Yesner G, Safari A, Maher A. Optimized design of layered bridge transducer for piezoelectric energy harvesting from roadway. Energy 2017;141:1133–45.

[25] Zhao Hongduo, Qin Luyao, Ling Jianming. Test and analysis of bridge transducers for harvesting energy from asphalt pavement. Int J Transp Sci Technol 2015;4:17–28.

[26] Kan J, Liu D, Wang S, Wang B, Yu L, Li S. A piezohydraulic vibration isolator used for energy harvesting. J Intell Mater Syst Struct 2014;25:1727–37.

[27] Wu Y, Ji H, Qiu J, Han L. A 2-degree-of-freedom cubic nonlinear piezoelectric harvester intended for practical low-frequency vibration. Sens Actuators, A 2017;264:1–10.

[28] Zhou S, Wang J. Dual serial vortex-induced energy harvesting system for enhanced energy harvesting. AIP Adv 2018;8:075221.

[29] Gusarov B, Gusarova E, Viala B, Gimeno L, Boisseau S, Cugat O, et al. Thermal energy harvesting by piezoelectric PVDF polymer coupled with shape memory alloy. Sens Actuators, A 2016;243:175–81.

[30] Huang HH, Chen KS. Design, analysis, and experimental studies of a novel PVDF-based piezoelectric energy harvester with beating mechanisms. Sens Actuators, A 2016;238:317–28.

[31] Li S, Crovetto A, Peng Z, Zhang A, Hansen O, Wang M, et al. Bi-resonant structure with piezoelectric PVDF films for energy harvesting from random vibration sources at low frequency. Sens Actuators, A 2016;247:547–54.

[32] Zhao X, Shang Z, Luo G, Deng L. A vibration energy harvester using AlN piezoelectric cantilever array. Microelectron Eng 2015;142:47–51.

[33] Fei C, Liu X, Zhu B, Li D, Yang X, Yang Y, et al. AlN piezoelectric thin films for energy harvesting and acoustic devices. Nano Energy 2018;51:146–61.

[34] Guido F, Qualtieri A, Algieri L, Lemma ED, De Vittorio M, Todaro MT. AlN-based flexible piezoelectric skin for energy harvesting from human motion. Microelectron Eng 2016;159:174–8.

[35] Płaczek M, Kokot G. Modelling and laboratory tests of the temperature influence on the efficiency of the energy harvesting system based on MFC piezoelectric transducers. Sensors 2019;19:1558.

[36] Gao F, Liu G, Chung BLH, Chan HHT, Liao WH. Macro fiber composite-based energy harvester for human knee. Appl Phys Lett 2019;115:033901.

[37] Ju S, Chae SH, Choi Y, Ji CH. Macro fiber composite-based low frequency vibration energy harvester. Sens Actuators, A 2015;226:126–36.

[38] Zhang X, Wang P, Liu X, Zhang W, Zhong Y, Zhao H, et al. Effect of post-annealing on microstructure and piezoelectric properties of ZnO thin film for triangular shaped vibration energy harvester. Surf Coat Technol 2019;361:123–9.

[39] Wang P, Du H. ZnO thin film piezoelectric MEMS vibration energy harvesters with two piezoelectric elements for higher output performance. Rev Sci Instrum 2015;86:075002.

[40] Kan J, Fan C, Wang S, Zhang Z, Wen J, Huang L. Study on a piezo-windmill for energy harvesting. Renewable Energy 2016;97:210–7.

[41] Cha Y, Chae W, Kim H, Walcott H, Peterson SD, Porfiri M. Energy harvesting from a piezoelectric biomimetic fish tail. Renewable Energy 2016;86:449–58.

[42] Hamlehdar M, Kasaeian A, Safaei MR. Energy harvesting from fluid flow using piezoelectrics: a critical review. Renewable Energy 2019;143:1826–38.

[43] Esu OO, Lloyd SD, Flint JA, Watson SJ. Feasibility of a fully autonomous wireless monitoring system for a wind turbine blade. Renewable Energy 2016;97:89–96.

[44] Hu Y, Yang B, Chen X, Wang X, Liu J. Modeling and experimental study of a piezoelectric energy harvester from vortex shedding-induced vibration. Energy Convers Manage 2018;162:145–58.

[45] Dai HL, Abdelkefi A, Wang L. Piezoelectric energy harvesting from concurrent vortex-induced vibrations and base excitations. Nonlinear Dyn 2014;77:967–81.

[46] Hobeck JD, Inman DJ. A distributed parameter electromechanical and statistical model for energy harvesting from turbulence-induced vibration. Smart Mater Struct 2014;23:115003.

[47] Danesh-Yazdi AH, Goushcha O, Elvin N, Andreopoulos Y. Fluidic energy harvesting beams in grid turbulence. Exp Fluids 2015;56:161.

[48] He X, Yang X, Jiang S. Enhancement of wind energy harvesting by interaction between vortex-induced vibration and galloping. Appl Phys Lett 2018;112:033901.

[49] Petrini F, Gkoumas K. Piezoelectric energy harvesting from vortex shedding and galloping induced vibrations inside HVAC ducts. Energy Build 2018;158:371–83.

[50] Mutsuda H, Tanaka Y, Patel R, Doi Y. Harvesting flow-induced vibration using a highly flexible piezoelectric energy device. Appl Ocean Res 2017;68:39–52.

[51] Li D, Wu Y, Da Ronch A, Xiang J. Energy harvesting by means of flow-induced vibrations on aerospace vehicles. Prog Aerosp Sci 2016;86:28–62.

[52] Truitt A, Mahmoodi SN. A review on active wind energy harvesting designs. Int J Precis Eng Manuf 2013;14:1667–75.

[53] Hobeck JD, Inman DJ. Artificial piezoelectric grass for energy harvesting from turbulence-induced vibration. Smart Mater Struct 2012;21:105024.

[54] Tsujiura Y, Suwa E, Nishi T, Kurokawa F, Hida H, Kanno I. Airflow energy harvester of piezoelectric thin-film bimorph using self-excited vibration. Sens Actuators, A 2017;261:295–301.

[55] Nieto AJ, Morales AL, Chicharro JM, Pintado P. An adaptive pneumatic suspension system for improving ride comfort and handling. J Vib Control 2016;22:1492–503.

[56] Morales AL, Nieto AJ, Chicharro JM, Pintado P. An adaptive pneumatic system for the attenuation of random vibrations. J Vib Control 2015;21:907–18.

[57] Spiroiu MA. Railway vehicle pneumatic rubber suspension modelling and analysis. Mater Plast 2018;55:24.

[58] Yin Z, Khajepour A, Cao D, Ebrahimi B, Guo K. A new pneumatic suspension system with independent stiffness and ride height tuning capabilities. Veh Syst Dyn 2012;50:1735–46.

[59] Soliman MSM, Abdel-Rahman EM, El-Saadany EF, Mansour RR. A wideband vibration-based energy harvester. J Micromech Microeng 2008;18:115021.

[60] Zhu Y, Zu J. A magnet-induced buckled-beam piezoelectric generator for wideband vibration-based energy harvesting. J Intell Mater Syst Struct 2014;25:1890–901.